AD-A053 832 NAVAL RESEARCH LAB WASHINGTON D C F/G 20/6
APPLICATION OF ADVANCED OPTICAL SPECTROSCOPIES TO THE STUDY OF --ETC(U)
FEB 78 J M SCHNUR, P E SCHOEN, R MILLER
UNCLASSIFIED NRL-MR-3709 SBIE-AD-E000 147 NL

OF
AD
A053832

END
DATE
FILMED
6 -78
DDC

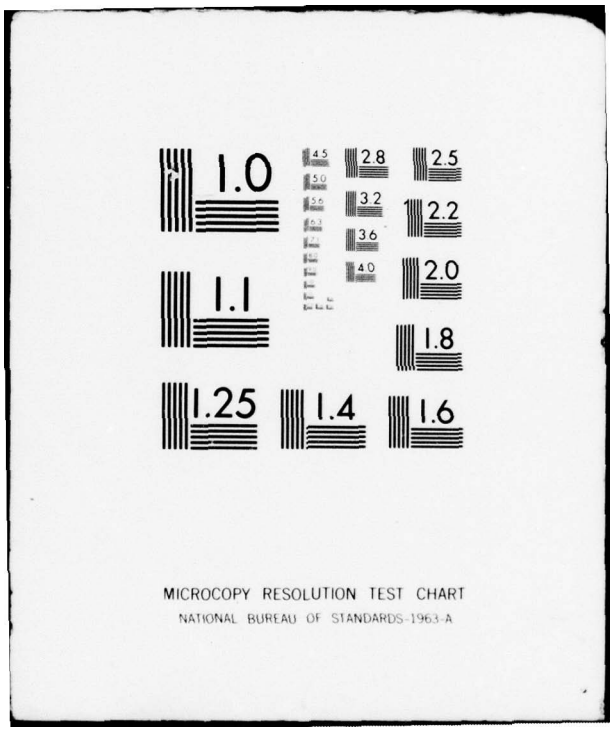
1.0
1.1
1.25
1.4
1.6
1.8
2.0
2.2
2.5
2.8
3.2
3.6
4.0
4.5
5.0
5.6
6.3
7.1
8.0
9.0
MICROCOPY RESOLUTION TEST CHART
NATIONAL BUREAU OF STANDARDS-1963-A

4/20

ade 000147

NRL Memorandum Report 3709

Application of Advanced Optical Spectroscopies to the Study of Energetic Materials

(12)

aett

Summary Report
1 October 1976 to 30 September 1977

J. M. SCHNUR

Optical Techniques Branch
Optical Sciences Division

February 1978

NAVAL RESEARCH LABORATORY
Washington, D.C.

SECURITY CLASSIFICATION OF THIS PAGE (When Data Entered)

REPORT DOCUMENTATION PAGE

READ INSTRUCTIONS BEFORE COMPLETING FORM

(14) 1. REPORT NUMBER: NRL -MR- 3709

2. GOVT ACCESSION NO.

3. RECIPIENT'S CATALOG NUMBER

(6) 4. TITLE (and Subtitle): APPLICATION OF ADVANCED OPTICAL SPECTROSCOPIES TO THE STUDY OF ENERGETIC MATERIALS ~~SUMMARY REPORT 1 OCTOBER 1976 TO 30 SEPTEMBER 1977~~

5. TYPE OF REPORT & PERIOD COVERED: Interim report on a continuing NRL problem

6. PERFORMING ORG. REPORT NUMBER

(10) 7. AUTHOR(s): J. M. Schnur, P. E. Schoen, R. J. Miller, C. J. Montrose, J. P. Sheridan

8. CONTRACT OR GRANT NUMBER(s): N00014-77WR70097; NR 092-552

9. PERFORMING ORGANIZATION NAME AND ADDRESS: Naval Research Laboratory, Washington, D.C. 20375

10. PROGRAM ELEMENT, PROJECT, TASK AREA & WORK UNIT NUMBERS: NRL Problem C07-11

11. CONTROLLING OFFICE NAME AND ADDRESS: Office of Naval Research, Arlington, Virginia 22217

(11) 12. REPORT DATE: February 1978

13. NUMBER OF PAGES: 83 (22) 177p.

14. MONITORING AGENCY NAME & ADDRESS (if different from Controlling Office)

15. SECURITY CLASS. (of this report): UNCLASSIFIED

15a. DECLASSIFICATION/DOWNGRADING SCHEDULE

16. DISTRIBUTION STATEMENT (of this Report)

Approved for public release; distribution unlimited.

(1) Summary rept. 1 Oct 76-30 Sep 77,

17. DISTRIBUTION STATEMENT (of the abstract entered in Block 20, if different from Report)

(16) RR024 02 (17) RR024 02 02

(18) SBIE (19) AD-E000 247

18. SUPPLEMENTARY NOTES

19. KEY WORDS (Continue on reverse side if necessary and identify by block number)

Energetic materials
Spectroscopy
Optical techniques

20. ABSTRACT (Continue on reverse side if necessary and identify by block number)

This report contains a detailed description of the research performed during the past year under Contract #N00014-77WR70097 Project Number 092-552. This series of papers reflect the substantial progress accomplished. This research program has been investigating the applicability of advanced optical techniques to the study of complex material problems associated with high energy substances. The report consists of a series of papers which reflect the substantial progess accomplished.

→ Those include: (see p. iii)

DD FORM 1 JAN 73 1473 EDITION OF 1 NOV 65 IS OBSOLETE
S/N 0102-014-6601

SECURITY CLASSIFICATION OF THIS PAGE (When Data Entered)

251 950

(cont fr p c)

CONTENTS

APPLICATION OF ADVANCED OPTICAL SPECTROSCOPIES TO THE STUDY OF ENERGETIC MATERIALS
SUMMARY REPORT
1 October 1976 to 30 September 1977

INTRODUCTION

This report contains a detailed description of the research performed during the past year under Contract #N00014-77WR70097 Project Number 092-552. This series of papers reflect the substantial progress accomplished. This research program has been investigating the applicability of advanced optical techniques to the study of complex material problems associated with high energy substances. In pursuit of this objective we have:

(a) Developed and perfected a high pressure Raman facility utilizing diamond anvil cell techniques;

(b) Completed design and fabrication of a multipass interferometric system to provide the capability of studying Brillouin spectra and thus obtaining. the viscoelastic characteristics of highly scattering materials such as rocket propellant binders;

(c) Established a digital correlation facility incorporating a Malvern digital auto-correlator;

(d) Completed microprocessor-computer construction and software development to ensure proper utilization of the sophisticated instruments described above;

(e) Utilized the Raman facility to study the effect of pressure upon conformational order in linear alkanes;

(f) Completed a critical analysis of the role of viscoelasticity measured by light scattering techniques in determining the structural integrity of rocket propellants;

(g) Initiated a study of the role of fast relaxation process in mechanisms of failure (fracture) in filled and unfilled polymeric materials.

These developments have resulted in several publications which are reproduced on the following pages.

Note: Manuscript submitted January 23, 1978

On the Possible Role of Viscoelasticity Measured by Light Scattering Techniques in Determining the Structural Integrity of Rocket Propellants

P. E. Schoen, J. M. Schnur

Naval Research Laboratory

R. Miller

Office of Naval Research

and

C. J. Montrose

The Catholic University of America

CONTENTS

I. Introduction

The detonation of a composite high energy material can develop from stable burning through convective burning in pores and cracks, to a possible low velocity explosion, and finally to a steady state detonation.[1] It is highly likely that the short-time viscoelastic properties (those which have time to react on the time scale of the mechanical and thermal loading) and their influence on the severity of fracturing play an important role in determining whether the material will, in fact, detonate. On the other hand the maintenance of the structural integrity of a solid propellant rocket engine over its lifetime requires that it resist creep deformation for periods of years. Thus the time scales of interest for viscoelastic response in propellants range from 10^{8} sec to less than 10^{-9} sec, an enormous span.

Recent advances[2-7] in Brillouin light scattering techniques make possible the measurement of the moduli of real polymeric binders in the time regime $\leq 10^{-8}$ sec, i.e. the short time regime which could only be reached for these materials by extrapolation or by time-temperature superposition methods previously. We propose in this paper that this powerful new technique be used to help determine the submicrosecond properties of explosives and propellants which could not be obtained in the past.

II. Fracture of Composite Materials

An ideal high energy composite material would respond to a stimulus by changing shape without crack formation and in so doing absorb the energy input viscously throughout its bulk. In other words, deformation in

in lieu of fracture is desirable to minimize the rate of new surface formation. In order to preclude fracture of the material the stresses generated in it as the load is applied must continually be relaxed so that the stress level at which cracking begins is not exceeded. In addition it is desirable that cracks that are initiated should propagate slowly, absorbing a maximum of energy as they grow. Key factors determining the rate of new surface creation are (1) the short time dependence of the viscoelastic properties of the binder and of its interface with the explosive particles and (2) the relative dimensions of the particles and the interspersed binder.

One can reckon the "short times" of importance for propellants to be on the order of 10^{-9} seconds. This estimate is obtained by computing the ratio of the dimension of a tip of a crack to the rate of crack propagation.[8] The crack tip dimension is on the order of 10^{-6} meter (approximate thickness in some cases of the plasticized binder between the oxidizer or propellant particles). Crack velocities vary in the low range from 10^{-7} m/sec to 10^{-2} m/sec, and in the high range in high pressure impacts to hundreds of meters/sec. Therefore information about stress relaxation processes occurring on the 10^{-9} second time scale is of obvious importance to binder deformation mechanics.

For unfilled polymers, stress relaxation data have been measured or extrapolated in the time scale from 10^{-10} seconds to 10^{7} seconds as illustrated by Ferry.[9] A typical shear or elongation modulus for a lightly crosslinked amorphous polymer is reproduced in Fig. 1 for

illustration. This curve was obtained by Ferry by utilizing time - temperature superposition on moduli obtained by three different investigators.

Stress relaxation data for a composite modified double base propellant[10] is also plotted on the same graph. At long times (10^5 seconds) the composite propellant is as stiff as the lightly cross-linked amorphous polymer; at shorter times (~ 10^{-2} sec) it is stiffer. Because short time experimental data are lacking, the propellant curve presented on the log-log plot has been extrapolated linearly to a glassy modulus of 10^{10} dynes/cm^2. However, extrapolation of data over so many decades into the transition region between rubbery and glasslike behavior is risky.

This is especially true in plasticized systems in which stress relaxation due to the presence of the plasticizer is important. In reality the time dependent properties of a composite propellant and a neat cross-linked polymer cannot legitimately be directly compared because of the relatively high modulus filler incorporated in the propellant. Bulk propellant material property data such as are given in Fig. 1 are used in continuum fracture mechanics analyses in which the bulk is treated as if its properties did not vary from one volume element to another.[8] However a composite propellant is not a homogeneous material. Clearly the continuum approach could fail in this case because mechanical properties and fracture mechanisms will change discontinuously from one volume element containing a solid particle to the next element containing binder

material. Cracks must successively propagate through binder, or around particles, or through particles. The macroscopic crack propagation process is therefore most likely dependent upon a rapid succession of individual microscopic processes each of which is dependent upon the spatially varying material properties (some of which are time and history dependent) of the specific volume element being stressed. To better understand and control the high rate mechanical properties, i.e. the tendency for cracks to initiate and propagate through the bulk, it may be necessary to understand the micromechanics of the particle - interface - binder system for which one will have to have obtained short time viscoelasticity data for the mixed components.

Regardless of which approach is used, continuum or micromechanics, measurement of the short time stress relaxation properties of the binder and of the particle-binder interface is necessary to provide data to fracture mechanics analyses and to correlate gross macroscopic fracture behavior with binder properties. It would be highly desirable (a) to provide short time data at the temperature of use and thereby avoid time-temperature superposition, (b) to eliminate destructive mechanical testing, and (c) to determine the effects of aging and thermal cycling upon short time behavior. It is the goal of this paper to suggest that Brillouin light scattering can make significant contributions toward achieving these ends.

III. Principles of Brillouin Scattering

The techniques of Brillouin and correlation light scattering spectroscopy have been used in the past decade to produce great advances in our understanding of the viscoelastic behavior of solids and fluids over the time range from 10 sec to 10^{-11} sec. [2,11-17]

Brillouin scattering is inelastic scattering of light from thermally induced density fluctuations (thermal "sound waves") in a sample.

The heat stored in a sample at room temperature makes its constituent molecules vibrate in a random fashion, causing some of them to move close together occasionally - a local, purely random compression. This compression causes the local temperature and density to rise momentarily before the molecules move apart again.

The relief of the compression can be regarded as a three-fold process in which the excess heat is conducted away (thermal diffusion) and the excess density is relaxed by the radiation of sound waves (just as water waves radiate from a pebble dropped into a pond) and by exchange of energy between translational molecular motions and internal molecular vibrations ("relaxation"). Sound wave generation, heat diffusion and energy relaxation are random processes which occur continuously and spontaneously in any warm object. There is no need to inject sound waves - they are always there. They cover the entire frequency range and travel in all directions simultaneously.

In the typical Brillouin experiment a laser beam of a single frequency f_o and well-defined momentum $\bar{k}_o$ is shone upon a sample. The

excitations in the sample cause some of the incident light to be scattered away from the laser beam in such a fashion that the scattered light carries information about the dynamics of the sample.

Just as X-rays are Bragg reflected by the planes of a crystal, light is Brillouin scattered in a specific direction by plane sound waves of a specific wavelength, and because the sound waves are moving the scattered light is doppler shifted in frequency by an amount f which is proportional to the velocity of sound. The process of heat diffusion and energy relaxation also cause light scattering. Since diffusion and relaxation are not traveling wave phenomena, the scattered light is not doppler shifted in frequency but is merely broadened about the incident frequency f_o by amounts proportional to the rates of diffusion and relaxation.

A typical experimental set-up is shown in Fig. 2. A laser beam with frequency f_o is directed onto a sample, and the light scattered at an angle θ with respect to the incident beam is collected and sent through an interferometer. The interferometer analyzes the scattered light into its respective frequencies. Sound of every frequency and propagation direction is present in the sample but only sound waves of a specific wavelength and propagating in the direction shown will scatter light into the interferometer because only they obey the Bragg condition. This condition (which is the momentum conservation law) and the energy conservation law are illustrated in Fig. 2 and the equations below.

$$\bar{q} = \bar{k}_o - \bar{k}_1 \qquad \text{(momentum conservation)} \qquad (1)$$

$$f = f_o - f_1 \qquad \text{(energy conservation)} \qquad (2)$$

where $q = 2\pi/\lambda$, λ being the wavelength of the sound wave satisfying the Bragg condition. Here a bar over a quantity indicates that it is a vector. f is the sound frequency, f_o and f_1 are the frequencies of the incident and scattered light, $\bar{q}$ is the momentum of the sound wave, and $\bar{k}_o$ and $\bar{k}_1$ are the momenta of the incident and scattered light.

Since the momenta are vector quantities they form a vector triangle as shown in Fig. 2. From this triangle is deduced the relation between the magnitudes of the momenta:

$$|k_o| \approx |k_1| \qquad (3)$$

$$q = 2k_o \sin(\theta/2) \qquad (4)$$

$$= 2\frac{n\pi}{\lambda_o} \sin(\theta/2)$$

where λ_o is the wavelength of the incident laser light and n is the index of refraction of the sample. q depends directly upon the scattering angle θ. Thus one can vary the wavelength and frequency of sound one observes by varying θ.

A model of a Brillouin spectrum is shown in Fig. 3. The narrow spectral line in the center is due to light scattered at the incident laser frequency, f_o, by the heat diffusion mode of the sample. The width of this line is proportional to the thermal conductivity, κ. (The central peak usually also contains light scattered by dirt and imperfections in the sample. The apparent linewidth in this case is that of the instrument.) Under certain conditions there is another spectral feature centered at f_o (indicated by the dotted curve in Fig. 3) caused by the

relaxation process, named the Mountain mode.[18] It has a width inversely proportional to the relaxation time τ, and is not seen unless the relaxation frequency, $1/\tau$, is less than the Brillouin frequency. On each side of the central feature, there are two peaks, doppler shifted up or down in frequency from f_o (produced by sound waves running toward or away, respectively, from the interferometer). These are peaks produced by longitudinal and shear sound waves, the shear wave causing the smaller frequency shift. Each peak has a width which is due partly to broadening by the interferometer and partly to the finite lifetime of the density fluctuations causing scattering ... the shorter the lifetime the broader the peak. A more detailed account of Brillouin scattering is given in the appendix of this paper.

IV. Measuring Material Properties

The excitations present in a sample - the sound waves, heat diffusion and energy relaxation - depend critically upon the material properties in which we are interested: particularly the sound velocity and absorption, which are functions of the real and imaginary parts, respectively, of the viscoelastic moduli, and the relaxation time which determines how quickly a substance can adjust to stress.

In a Brillouin scattering experiment one measures f, the frequency of sound having momentum q. The proportionality constant between q and f is the velocity of sound, v.

$$f = qv/2\pi \qquad (5)$$

Once the velocities have been measured the real parts of the longitudinal modulus, M', and the shear modulus, G', can be calculated from the relations:

$$M' = \rho \nu_L^2 \tag{6}$$

$$G' = \rho \nu_s^2 \tag{7}$$

ρ is the density and ν_L and ν_s are the longitudinal and shear sound velocities.

Similarly from the longitudinal and shear Brillouin linewidths, Γ_ℓ and Γ_s (half widths at half maximum), the imaginary parts M'' and G'' can be determined:

$$M'' = 2\pi\rho \frac{\nu_L}{q} \Gamma_L \tag{8}$$

$$G'' = 2\pi\rho \frac{\nu_s}{q} \Gamma_s \tag{9}$$

The compressional modulus, K, can then be found from the relationships:

$$K' + \frac{4}{3} G' + i (K'' + \frac{4}{3} G'') = M' + iM'' \tag{10}$$

G, M, ν_L and ν_s are, in general, frequency dependent parameters. For Brillouin scattering experiments the frequency is of the order of 10^9 Hz, giving what are, effectively, the infinite frequency values G_∞, M_∞, $\nu_{s\infty}$ and $\nu_{L\infty}$ for most solid non-viscoelastic materials. In those cases in which these parameters exhibit a frequency dependence in this range however, Brillouin scattering can determine this important functional relationship.

As mentioned earlier the molecules of a material are constantly in motion. These motions include not only the external translational vibrations which produce sound waves but also internal oscillations of

individual atoms against each other within the molecules. The internal and external degrees of freedom can, given enough time, exchange energy among themselves, and this exchange has a marked effect on the thermodynamic and viscoelastic properties of the material. In solids the time required for the interchange of energies is typically of the order of microseconds or longer. Therefore properties of the material measured at megahertz or lower frequencies tend to be dispersive - that is, they have different values at different frequencies. In the gigahertz frequency domain of Brillouin scattering most solids(though not all) are not dispersive. The time scale is too short in this domain for energy exchange to take place and the properties measured have their high frequency or "infinite" frequency limiting values.

For fluids on the other hand the Brillouin frequency range is often dispersive and much effort has been devoted to the study of relaxation times (the time for energy exchange to take place) in gases and liquids of different types.[5]

In the borderline case of the viscoelastic materials Brillouin techniques have determined a relaxation time for a few materials such as polymethyl acrylate at frequencies of 10-100 GHz.[19]

The type of effect relaxation has on material properties is shown in Fig. 4 for the velocity of sound and the bulk viscosity. In the case of the Figure there are two relaxation times, τ_1, and τ_2. For each value of τ these curves have the form:

$$\frac{v_o^2}{v^2} = 1 - \left(\frac{v_\infty^2 - v_o^2}{v_\infty^2}\right)\left(\frac{\omega^2 \tau^2}{1+\omega^2\tau^2}\right) \qquad (11)$$

$$\eta = \left(\frac{\nu_\infty^2 - \nu_o^2}{1+\omega^2\tau^2}\right)\rho\tau \qquad (12)$$

ω is $2\pi f$ and the subscripts o and ∞ indicate the lower and higher frequency values of the velocity.

More complex materials may have many relaxation times - and are best described by a relaxation function, a distribution of relaxation times. The many different paths and time scales for the redistribution of energy among the different degrees of freedom of complex materials have a very strong influence on their behavior under different types of stress. The two curves in Fig. 5 illustrate relaxation functions for liquids which have the same low frequency, long time scale viscosity. It is apparent that there are marked differences in the short time response characteristics of the two substances; methylphenylsiloxane polymer will quickly relax a substantial portion of a suddenly applied stress whereas the polyphenyl ether will not.

This is the kind of information that would be of great use in evaluating and selecting polymeric binders. In some substances the Brillouin technique may be sufficient to determine a large part of the relaxation function; it will at a minimum provide the high frequency values which can be combined with low frequency or long time measurements made by other techniques.

These measurements should be able to be performed on real binder systems. The ability of Brillouin scattering to deal with "real" materials of poor optical quality is a relatively recent development. Generally the interferometer which is used to sort out light of different frequencies is a low "contrast" instrument; that is, it has difficulty

separating spectral components whose intensities differ by a ratio of 10^3 or more. The imperfections in many materials scatter light very strongly and mask the signal one wishes to see. The recently perfected technique of "multipassing" in which scattered light is sent through the interferometer 3 or 5 times in succession improves the contrast ratio from 10^3 to 10^9 or better. Now, materials such as metals, thin films, epoxies, rubbers, opaque polymers, and so forth, have been examined by Brillouin scattering successfully - whole classes of materials that were impossible to work with 5 or 10 years ago. However, few examples of these experiments have appeared in the literature as yet because the technique is so new. It is highly desirable that work along these lines be done in the near future. It is becoming quite clear that optical scattering investigations offer the most promising experimental approach for the viscoelastic characterization of propellant binder systems; such characterization studies are an invaluable aid (perhaps an essential one) in the development of safe high energy materials.

APPENDIX on Brillouin and Correlation Spectroscopy

The spectrum that one observes in scattering from density fluctuations can be understood in terms of a few simple considerations. In any system (considered to be homogeneous on a macroscopic scale) the random thermal motion of the constituent molecules results in microscopic nonuniformities or fluctuations. In particular at any instant there are regions where the density is higher (local compression) or lower (local rarefactions) than the average density ρ_o. Examine one such region where at some instant (say $t = 0$) there exists a local compression. As time evolves the behavior in this region will be such as to return the density to its equilibrium value.

Before detailing the specifics of how this dynamical return to equilibrium influences the spectrum, one important point regarding the density fluctuation-light scattering process itself must be made. The intensity and spectral distribution of the light scattered through an angle θ are determined by the $\vec{q}^{th}$ Fourier spatial component (wavelength $\Lambda = 2\pi/q$) of the density considered as a function of position. The meaning of this result can be appreciated by considering the sketches shown in Fig. 6. The random variation of the density can be written as a superposition of sinusoidal curves of various wavelengths each with its own amplitude and phase. The scattering observed at any angle θ depends only on one of these sinusoids -- that with wavelength $\Lambda = 2\pi/q$.

The spectrum that is observed is thus determined by the time dependent behavior of a density variation, the spatial dependence of which is of the

form $e^{\pm i\vec{q}\cdot\vec{r}}$. This time dependence can be sorted into three fundamental dynamical "modes" that are available to relax the density fluctuation. These modes are thermal diffusion, sound wave propagation, and structural relaxation. Each of these leaves its characteristic signature in the scattered light spectrum.

Thermal Diffusion

Associated with a density variation in a material there is a corresponding energy variation. The latter is relaxed via the conduction of heat away from the regions of higher temperature. The concomitant relaxation of the density proceeds exponentially in time at a rate determined by the thermal conductivity κ. Specifically the decay goes as

$$\exp(-\kappa q^2 t/\rho_o C_p) \tag{A1}$$

where C_p is the specific heat. Because this is a non-propagating (i.e. non-oscillatory) phenomenon, it results only in a frequency broadening of the scattered light frequency, f_o. This is illustrated in Fig. 8a. The spectral component associated with thermal diffusion is the so-called Rayleigh line; the amount of the broadening (the Rayleigh half-width) is

$$\Gamma_R = \kappa q^2/\rho_o C_p \tag{A2}$$

which is typically on the order of 10^6 to 10^7 Hz.

Sound Wave Propagation (Brillouin Scattering

A local compression or rarefaction in a medium leads inevitably to the radiation of sound waves. If the disturbance, i.e. the density variation, is spatially sinusoidal with wavelength Λ, the resulting sound waves are

characterized by a definite frequency, f, and propagate with a speed $v = f\Lambda$. These thermally generated sound waves (phonons) thus appear as moving diffraction gratings, scattering light in the direction θ determined by the Bragg condition. Because the wave is moving, the scattered light is doppler shifted in frequency by an amount $\pm f$. Thus the spectrum contains a Brillouin doublet symmetrically placed about the incident light frequency as shown in Fig. 7a. The width of the Brillouin lines is determined by the sound attenuation coefficient α (which governs the temporal decay of the propagating fluctuation); specifically

$$\Gamma_B \simeq \alpha v/2\pi. \tag{A3}$$

Typically the Brillouin shift frequencies are on the order of 10^9 to 10^{10} Hz; since this represents oscillations on a time scale quite short compared with that required for heat flow, the sound speed that determines these shifts is related to $M(\omega_B)$, the <u>adiabatic</u> longitudinal modulus of the medium at the angular frequency $\omega_B = 2\pi f$. In particular,

$$M(\omega_B) = \rho_o v^2. \tag{A4}$$

Under certain circumstances the depolarized spectrum, e.g. incident light polarization perpendicular to the scattering plane and scattered polarization in the scattering plane, will exhibit a similar doublet structure. These components arise from scattering from transverse waves in the medium which propagate at a speed v_T. This is related to $G(\omega_T)$, the shear modulus at the angular frequency $\omega_T = 2\pi v_T/\Lambda$ by

$$G(\omega_T) = \rho_o v_T^2. \tag{A5}$$

Structural Relaxation

In a non-crystalline medium a local increase in the density occurs via two mechanisms: (1) a decrease in the intermolecular spacings; and (2) a rearrangement of the local structure. The return of the density of its equilibrium value thus requires the relaxation of these two mechanisms. The former occurs essentially instantaneously (upon removal of the stress that produced the compression) while the latter structural relaxation process proceeds at a finite rate characterized by the structural relaxation time τ. Generally speaking, the structural relaxation dynamics are not described by a simple exponentially decaying function of time, but rather are characterized by some more complicated relaxation function, $\phi(t)$*. This function is closely allied to the frequency dependent modulus $M(\omega)$ and viscosity $\eta(\omega)$ familiar from viscoelastic theory through a Fourier transform relationship:

$$M(\omega) + i\omega\eta(\omega) = M_o + M_r\, i\omega\int_o^\infty dt\; e^{-i\omega t}\phi(t) \qquad \text{(A6)}$$

where M_o is the equilibrium bulk modulus of the system and M_r is the relaxational part of the modulus.

The effect of structural relaxation on the light scattering spectrum is rather different depending on the rate at which the relaxation process occurs. We distinguish three cases.

*In this discussion $\phi(t)$ is normalized such that $\phi(0) = 1$ and $\phi(t\to\infty) = 0$. The structural relaxation time is defined by

$$\tau = \int_o^\infty dt\; \phi(t).$$

Case I. $1/\tau >> \omega_B$. Here the structural rearrangements proceed rapidly ($\tau \lesssim 10^{-11}$ sec) compared with the period of the thermal sound waves. Consequently, the structural changes remain in phase with these oscillations and they contribute only to the Brillouin components in the spectrum; there is no separate spectral feature corresponding to the structural relaxation process. The Brillouin shift frequencies reflect the eqilibrium longitudinal modulus of the system, M_o.

Case II. $\omega_B >> 1/\tau >> \kappa q^2/\rho_o C_p$. Because it proceeds rapidly compared with the rate of thermal diffusion, the structural relaxation of the density fluctuation is an adiabatic process. However, because the structural changes equilibrate slowly in comparison with the oscillation of the phonon modes, they cannot contribute to the Brillouin lines in the spectrum. Rather (Fig. 7b) they constitute the so-called Mountain component in the spectrum which (since the structural changes are nonpropagating) is centered at the incident light frequency. The spectral shape of this component $S(\omega)$ is given by

$$S(\omega) \simeq \frac{\eta(\omega)}{[\omega\eta(\omega)]^2 + M(\omega)^2} ; \qquad (A7)$$

the halfwidth of this line is approximately:

$$\Gamma_m \sim 1/\tau. \qquad (A8)$$

Consequently in this case the viscoelastic relaxation function $\phi(t)$ can be inferred from the Mountain component while the Brillouin shifts yield the "infinite frequency" or solid-like modulus

$$M_\infty = M_o + M_r = \rho_o v_\infty^2. \qquad (A9)$$

Case III. $\omega_B >> \kappa q^2/\rho_o C_p >> 1/\tau$. Here the viscoelastic relaxation occurs quite slowly compared with the thermal diffusion rate; as a result the structural dynamics reflected in the Mountain component -- which is here much narrower than the Rayleigh line (Fig. 7c) -- are isothermal rather than adiabatic. The form of the spectrum is similar to that given for $S(\omega)$ above if $\eta(\omega)$ and $M(\omega)$ are interpreted as isothermal quantities.

Experimentally the measurement of the spectrum in Cases I and II, as well as the measurement of the depolarized transverse doublet is conveniently carried out using a flat-plate Fabry-Perot interferometer as the spectrum analyzer. This situation is sketched in Fig. 2. Practically speaking the range of scattering vectors q that can be probed (by varying the scattering angle and/or using different incident wavelengths) is

$$0.12 \times 10^5 \text{ cm}^{-1} \lesssim q \lesssim 2.5 \times 10^5 \text{ cm}^{-1}$$

corresponding to a wavelength range

$$0.25 \text{ μm} \lesssim \Lambda \lesssim 5 \text{ μm}.$$

Similarly the frequency range over which the spectrum can be measured is roughly from 10^7 to 10^{12} Hz, the upper limit being set by practical considerations on the spacing of the plates, while the lower limit represents the frequency resolution that can be maintained on a Fabry-Perot interferometer.

In the situation described above as "Case III," the Brillouin lines can be measured using Fabry-Perot spectroscopy, but the Mountain component -- containing the dynamical relaxation information -- is clearly too narrow ($\Gamma_M \lesssim 10^6$ Hz) to be studied in this way. In this case the use of digital time correlation spectroscopy has been demonstrated to be a useful tool

for obtaining this information (from relatively "clean" samples, optically speaking) on time scales of 10^{-6} to 10 sec (equivalent to a frequency range of about 0.1 to 10^6 Hz).[15,16,20] In this technique one allows the scattered light to fall directly on the photomultiplier tube (the spectrum analyzer is removed) and then using an electronic digital correlator analyzes the time correlation function, G(t), of the scattered light intensity. This is related to $\sigma(t)$, the Fourier transform of $S(\omega)$ by

$$G(t) = a + b\sigma(t)^2 \qquad \text{(A10)}$$

where a and b are constants determined by the experimental conditions.

References

1. A. F. Belysev, et al. "Transition from Deflagration to Detonation in Condensed Phases," National Technical Information Service #TT 74-50028 (1973) Chapter 5.

2. "Proceedings of the 2nd International Conference on Light Scattering in Solids," M. Balkanski, ed., (Flammarion, 1971, Paris).

3. J. R. Sandercock, Opt. Comm. 2, 73 (1970).

4. J. R. Sandercock, Phys. Rev. Letters 28, 237 (1972).

5. J. R. Sandercock, Phys. Rev. Letters 29, 1735 (1972).

6. Q. H. Lao, P. E. Schoen, B. Chu, Rev. Sci. Inst. 47, 418 (1976).

7. D. S. Bedborough and D. A. Jackson (to be published) J. Phys. E (GB).

8. W. G. Knauss, International J. of Fracture Mech. 6, 7 (1970).

9. J. D. Ferry, "Viscoelastic Properties of Polymers ," (Wiley, 1970, New York).

10. H. B. Deweese, "Polaris A-3 Second Stage Fleet Motor Analysis," Hercules Report R/C 2-77-93, Aug. 1973. Referenced in: S. W. Beckwith and D. T. Wang, "Crack Propagation in Double Base Propellants," JANNAF Structures and Mechanical Behavior Working Group, 14th Meeting, 15-17 Feb.1977, CPIA Publication 283, April 1977.

11. H. Z. Cummins in "Quantum Optics," Proceedings of the International School of Physics - Enrico Fermi, Course XLII (Academic Press, 1969, New York) ed. by R. J. Glauber, p.247.

12. W. L. Peticolas, G. I. A. Stegeman, and B. P. Stoicheff, Phys. Rev. Letters 18, 1130 (1967).

13. "Light Scattering Spectra of Solids," G. B. Wright, ed. (Springer-Verlag, 1969, New York).

14. P. A. Fleury and J. P. Boon in "Advances in Chemical Physics," Vol. XXIV (Wiley, 1973, New York), p.1.

15. C. Demoulin, C. J. Montrose, and N. Ostrowsky, Phys. Rev. A9, 1740 (1974).

16. J. F. Dill, P. W. Drake and T. W. Litovitz, ASLE Transactions 18, 202 (1975).

17. Q. H. Lao, P. E. Schoen, and B. Chu, J. Chem. Phys. 64, 3547 (1976).

18. R. D. Mountain, J. Res. Natl. Bur. Std. A70, 207 (1966).

19. Y. Y. Huang, E. A. Friedman, R. D. Andrews, and T. R. Hart, p.488 of ref. 2.

20. C. C. Lai, P. B. Macedo and C. J. Montrose, J. Am. Ceram. Soc. 58, 120 (1975).

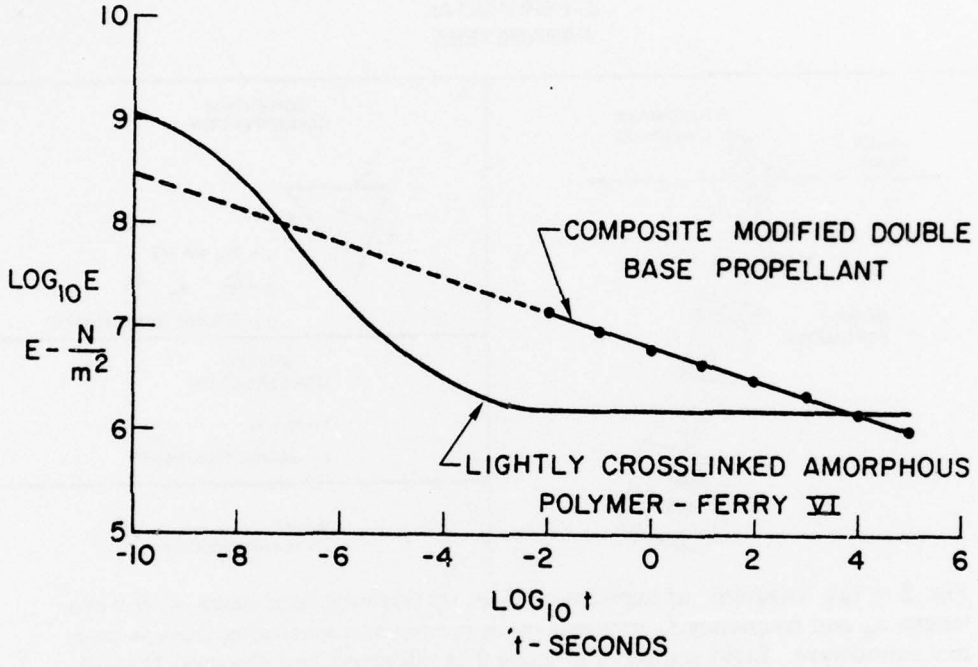

Fig. 1 — Elastic moduli of two materials vs. time: straight line is composite modified double base propellant (dotted position of line is extrapolation); curved line is lightly crosslinked amorphous polymer

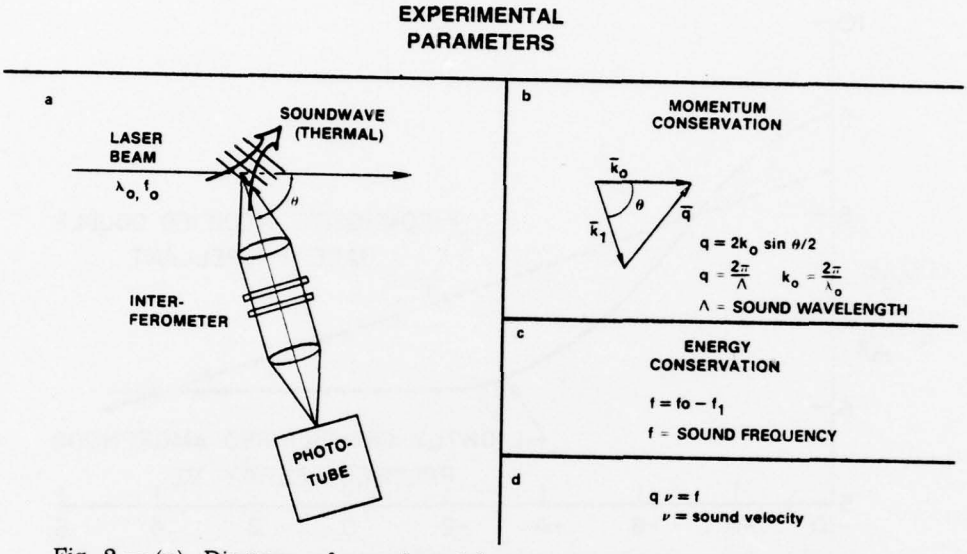

Fig. 2 — (a) Diagram of experimental set up showing laser beam with wavelength λ_o and frequency f_o incident upon sample and scattering from a thermal soundwave. Light scattered at angle θ is collected and directed through interferometer to phototube. (b) Scattering triangle for momentum conservation. (c) Energy conservation law. (d) Equation relating experimental parameters to sound velocity.

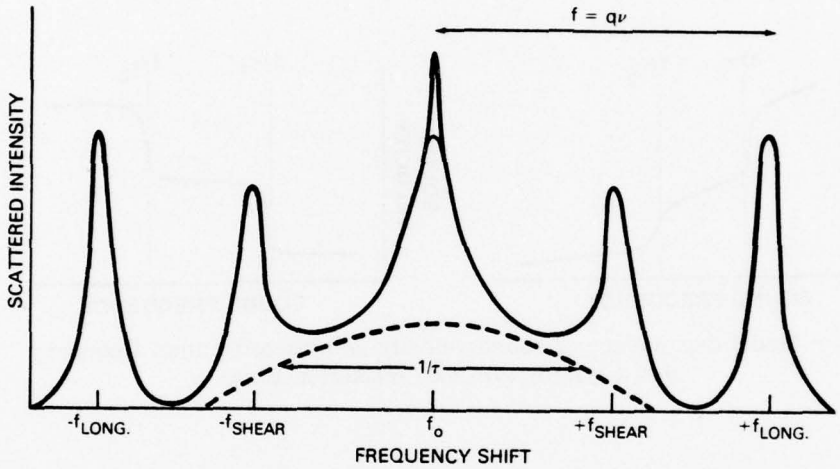

Fig. 3 — Model Brillouin spectrum. Central peak at incident laser frequency f_o is Rayleigh line (narrow peak at top is due to stray laser light). Neighboring peaks are up and down frequency shifted Brillouin lines due to longitudinal and shear sound waves. Dotted line is "Mountain" profile with frequency width $\sim 1/\tau$.

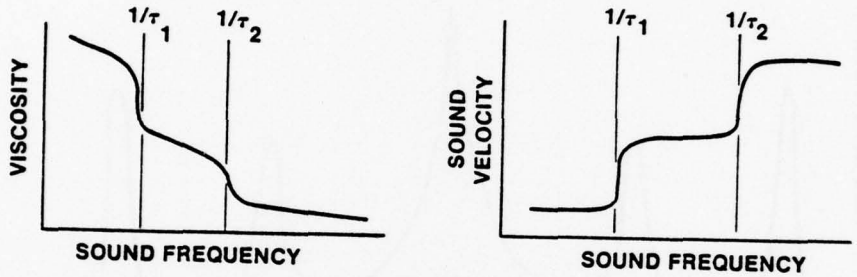

Fig. 4 — Model dependence of sound velocity and viscosity upon frequency for a system with two relaxation times

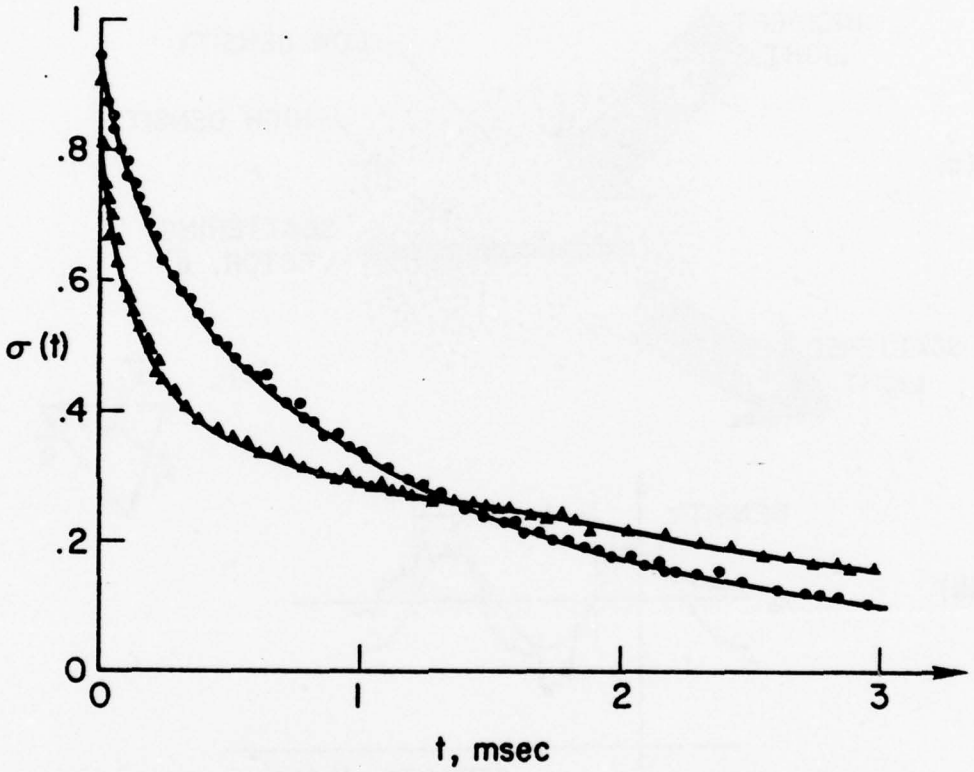

Fig. 5 — Measured correlation functions $\sigma(t)$ for a polyphenyl ether (5P4E) at 22°C, 1.2 kbar (0) and for a short chain methyl pehnylsiloxane polymer at 20°C, 2.1 kbar (4).

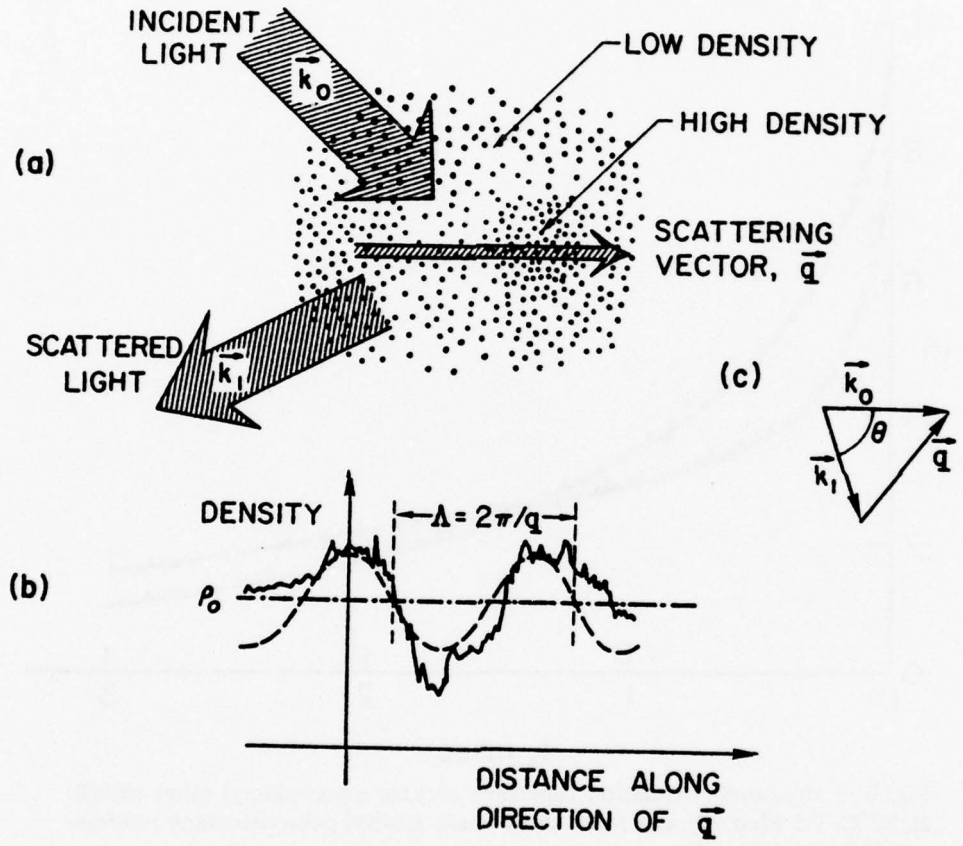

Fig. 6 — (a) Instantaneous configuration of molecules in the scattering volume showing low and high density regions. (b) The corresponding variation of the density along the direction of $\vec{q}$ (solid curve); the q^{th} Fourier component of this variation (broken curve) is shown superimposed on the average density (dash-dot curve). (c) The "scattering triangle."

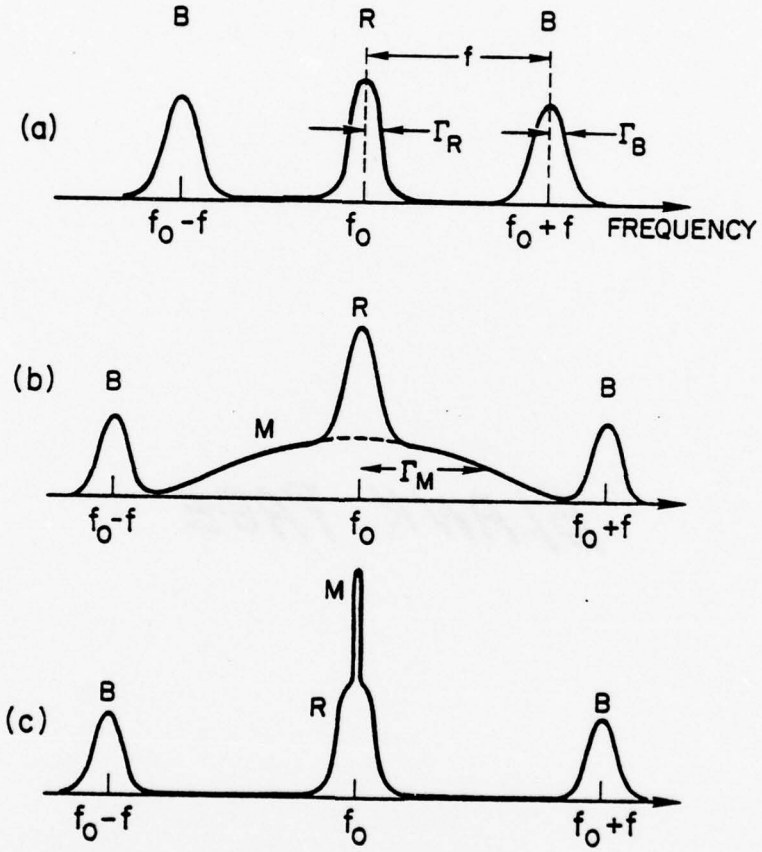

Fig. 7 — Spectrum of light scattered by a viscoelastic material. R labels the Rayleigh component, B the Brillouin components and M the Mountain component. The spectra (a), (b), and (c) correspond to the cases I, II, and III (in the text), respectively.

Techniques for Observing Weak Raman Signals in the Diamond Pressure Cell

P. E. SCHOEN, J. M. SCHNUR, and J. P. SHERIDAN

Naval Research Laboratory, Washington, D.C. 20375

Index Headings: **Light scattering; Spectroscopy, Raman; Instrumentation, high pressure; Techniques, spectroscopic.**

We wish to report a technique of using the 752.5 nm line of the Kr^+ laser to excite the Raman effect in weakly scattering samples in a gasketed diamond anvil pressure cell. The use of this near-infrared excitation substantially reduces the fluorescence of the diamond windows which otherwise tends to distort and overwhelm weak Raman signals. This excitation also reduces interference from the fluorescence of the ruby fragment placed in the cell for pressure measurement.[1] These are, we believe, the first spectra obtained from weak Raman scatterers in a diamond/ruby pressure cell.

The diamond anvil cell within recent years has rapidly been gaining acceptance as a tool for high pressure x-ray spectroscopy and microscopy[2] as well as optical spectroscopy.[3] The simplicity of the device and its relatively low cost make it quite attractive, particularly for applications in which the desired pressures are in excess of a few kilobars. For Raman scattering the advantages of the diamond cell include a large aperture (~f/1.8 in our case), ease of loading and manipulating the cell, simple temperature control, and quick measurement in situ of the pressure and pressure gradients in the sample by the ruby fluorescence method. A significant difficulty with the cell, however, is fluorescence caused by the incident laser beam passing through the diamonds. This fluorescence can be strong enough to distort or completely mask weaker Raman bands.[4] Our interest in this problem grew out of an effort to investigate the pressure and temperature dependence of the conformation of *n*-alkane molecules by monitoring the relative intensities of the low frequency ($< 600\ cm^{-1}$) "accordion mode" Raman bands. In the case of the small carbon-number alkanes these Raman bands are not particularly strong and the spectrum may easily be distorted by fairly low levels of fluorescence. However, to detect changes in molecular conformation, accurate quantitative measurements of the relative band intensities are required. In order to make such precise measurements possible we have taken two special measures to minimize the diamond and ruby fluorescence and thus improve signal/noise ratios in our data: first, we have employed one of the red lines (647.1, 676.4, or 752.5 nm) of a Kr^+ laser for the incident light, and second, we have paid careful attention to the scattering geometry of our setup which we describe below.

The use of red excitation significantly reduces fluorescence. In our case we are constrained to use the near infrared line at 752.5 nm because we are using the ruby fluorescence pressure measurement technique. In this technique we place a small fragment of ruby in the cell along with the sample and measure the frequency of the pressure sensitive fluorescence maximum of the ruby. This fluorescence is extremely strong and peaks at about 694 nm so that if the laser is operating at 647.1 or 676.4 nm the Raman spectrum is obscured even if the laser beam is only illuminating the ruby indirectly by light scattered from the cell windows.

If the laser is operated at 752.5 nm and the beam is not directly striking the ruby the fluorescence of the ruby and the diamond will be sufficiently weak that good quantitative intensity measurements can be made of spectra of weak Raman sources. Such a spectrum of normal C_7H_{16} is shown in Fig. 1. We can see the all-*trans* accordion band at 318 cm^{-1} (all the accordion bands shift to higher frequencies with increasing pressure) and four neighboring higher frequency bands due to kinked conformers.[5] All the bands have reasonably good signal/noise ratios and rise from a flat, relatively weak and featureless fluorescent background. (The large band near 1300 cm^{-1} is the diamond Raman line.) The intensity measurements are simple to obtain and do not require use of computer subtraction or fast Fourier transformations.

The spectrometer used here was a Spex 1401 double monochromator with holographic gratings peaked for performance between 600 and 900 nm. The detector was an RCA C31034 PM tube sensitive to about 900 nm, giving a Raman Stokes range of about 2000 cm^{-1}. Raman bands with higher frequency shifts can be detected if the

Received 22 February 1977; revision received 18 March 1977.

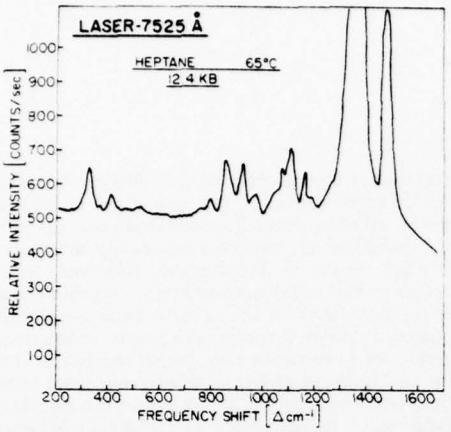

FIG. 1. Raman spectrum of C_7H_{16} at 65°C and 12.4 kbar pressure taken with 752.5 nm excitation in a diamond anvil pressure cell in the presence of a small ruby fragment. The strong band running off scale at 1330 cm^{-1} is the diamond Raman band. Spectrometer bandpass is 8 cm^{-1} (see indication of bandpass in Fig. 3).

laser is tuned to a shorter wavelength. The high frequency bands are far enough from the fluorescence peaks not to be obscured by them. The diamond anvil cell was of the Van Valkenberg[6] design and was supplied by High Pressure Diamond Optics. The diamonds were type II, specially selected for low fluorescence and optical use.

To obtain the spectrum in Fig. 1 the spectrometer was scanned with 8 cm^{-1} bandpass over a spectral range 200 to 1500 cm^{-1} in 14.5 h. The sample was held in a gasket of thickness 0.3 mm with a hole of diameter 0.3 mm. The laser beam power entering the diamond window of the pressure cell was about 120 mW. It was found that higher beam power caused appreciable sample heating, in one case melting a hole through a pressure frozen sample of a normal alkane.

The scattering geometry used is important in minimizing the amount of fluorescence observed. Our light collecting optics were arranged in a near-backscattering setup (Fig. 2). The laser beam was focused into the diamond cell 15° off normal incidence so that the specularly reflected beam missed the collecting lens. This reduced the strength of the Rayleigh line at low frequency shifts and allowed the image of the beam as it slanted through the diamond before reaching the sample to be partially blocked by the spectrometer slits. The slits were opened only enough to pass the image of the sample where the beam was passing through it. In this manner much of the laser induced diamond fluorescence was blocked from reaching the detector. Note from the inset in Fig. 2 that the pathlength of the laser beam through the diamonds is considerably greater than through the sample. This means that for 180° scattering the ratio of diamond to sample scattering volumes would be rather unfavorable.

For purposes of comparison we have taken another spectrum of C_7H_{16} (Fig. 3) under similar experimental conditions of temperature and pressure, off-normal incidence, scan time and laser power, this time using the green 514.5 nm excitation of an Ar^+ laser. The diamond fluorescence is strong and broad, extending out from a peak near the laser frequency for over 3000 cm^{-1}. The 318 cm^{-1} band is barely visible and the neighboring kinked-conformer bands cannot be seen in spite of the fact that these bands are several times stronger here than in the previous case. This is due to the fact that the fluorescence has increased much more than the Raman signal has. The signal/noise ratio of these bands has been reduced severely by the increase in the strength of the background. With an expanded vertical scale even some of the stronger alkane bands are difficult to see because of the sharp slant of the background. Only the strongest band at 1450 cm^{-1} stands out obviously from the fluorescence. However, this finding indicates that if one is interested in strong Raman scattering samples fluorescence from the diamond cell with the Ar^+ laser is tolerable.

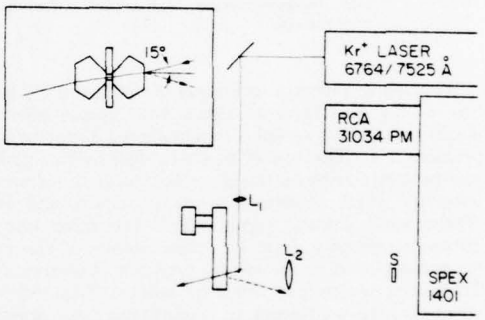

FIG. 2. Experimental set-up: laser beam is focused by lens L_1 into sample at 15° off-normal incidence. Scattered light is collected by lens L_2 and focused onto slits of spectrometer through polarization scrambler S. Dotted line shows specularly reflected light. Inset shows diamonds pressing against gasket hole in which sample is placed.

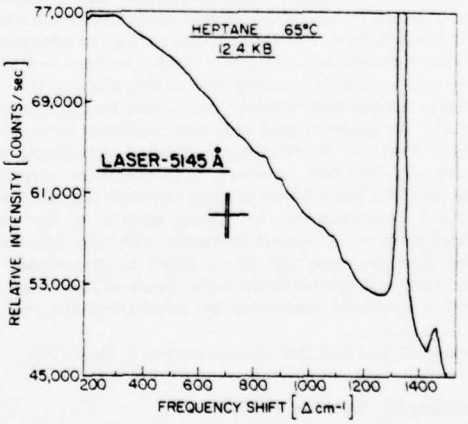

FIG. 3. Raman spectrum of C_7H_{16} at 65°C and 12.4 kbar pressure taken with 514.5 nm excitation in a diamond anvil pressure cell in the presence of a small ruby fragment. Spectrometer bandpass is indicated by vertical bars.

As mentioned earlier, this technique was developed during the course of a study of the liquid *n*-alkane which focused upon the pressure dependence of the longitudinal acoustic Raman modes of the all-*trans* and *gauche* conformations of the chain molecules. For a given temperature and pressure, the relative intensities of these accordion mode bands indicate the relative populations of molecules with different conformations. Our experimental results indicate that, surprisingly, as the pressure is increased on a short-chain liquid *n*-alkane, the number of kinked conformers increases relative to the number of straight-chain conformers, this in spite of the fact that the molecules freeze in the all-*trans* conformation. Subsequent to these observations we have developed a theoretical explanation for this effect based on an extension of Alben's[7] model of a dense fluid of hard rods interacting only through excluded volume effects and Van der Waals attraction. This model is in qualitative agreement with the observed effect and is the subject of another paper.[8]

In summary, we have shown here that use of the 752.5 nm Kr^+ laser line together with careful attention to the geometric details of the experimental set-up can allow quantitative Raman studies of weakly scattering materials to be conducted in the diamond anvil cell while the pressure is monitored by the ruby fluorescence technique.

---

1. J. D. Barnett, S. Block, and G. J. Piermarini, Rev. Sci. Instrum. 44, 1 (1973).
2. D. C. Bassett, S. Block, and G. J. Piermarini, J. Appl. Phys. 45, 4146 (1974).
3. B. A. Weinstein and G. J. Piermarini, Phys. Lett. 48A, 14 (1974); D. M. Adams and S. K. Sharma, *Proceedings of the Fifth International Conference on Raman Spectroscopy*, University of Freiburg, E. M. Schmid, Ed. (Schulz, Freiburg, 1976) p. 756.
4. D. M. Adams, S. J. Payne, and K. Martin, Appl. Spectrosc. 27, 377 (1973).
5. R. F. Schaufele, J. Chem. Phys. 49, 4168 (1968).
6. C. E. Weir, E. R. Lippincott, A. Van Valkenberg, and E. N. Bunting, J. Res. Natl. Bur. Stand. 63A, 55 (1959).
7. R. Alben, Mol. Cryst. Liq. Cryst. 13, 193 (1971).
8. P. E. Schoen, R. Priest, J. M. Schnur, and J. P. Sheridan, (to be published).

Raman Study of Conformational Characteristics of Chain Molecules under High Pressure

P. E. Schoen, R. Priest, J. P. Sheridan and J. M. Schnur
Naval Research Laboratory
Washington, D. C. 20375

Introduction

As part of a continuing program to study the properties of lubricants and polymers, we have undertaken an investigation of the conformational properties of linear alkanes and polymers as functions of temperature and pressure. We have successfully obtained the Raman spectra of these materials in the range of 1-20 kbar from a gasketed diamond anvil cell while calibrating the pressure with the ruby fluorescence technique.[1] The conformations of heptane (C_7H_{16}) and hexadecane ($C_{16}H_{34}$) have been monitored by the observation of conformationally sensitive Raman bands. Our data indicate that heptane becomes more "kinked" (more gauche bonds) as a function of pressure. This result was surprising to us at first, since at sufficiently high pressure, heptane freezes in the unkinked, all trans conformation. We have developed a theory based on excluded volume considerations which is consistent with these observations.

Since the Raman signal from the alkanes was relatively weak and the fluorescence background of diamond[2] and ruby was strong, we have had to employ near infrared laser excitation and also pay careful attention to scattering geometry in order to obtain useful spectra. These techniques will be described elsewhere.[3]

We have benefitted in this study from the large amount of work that has been done on the normal mode analysis of the alkanes and polyethylene.[4]

From model calculations and Raman and infrared spectroscopic investigations at room pressure the vibrational frequencies of the different normal modes of the alkanes have been identified for the straight chain, all-trans configuration as well as for some of the kinked, gauche conformers. There are three frequency ranges of interest to us: 200-550, 1060-1140, and 2800-3000 cm^{-1}. In the low frequency region of the Raman spectrum the alkanes have bands known as the longitudinal acoustic modes (LAM) which are cuased by accordian-like vibrations of the molecules along their lengths.[5] These vibrations have frequencies which are inversely proportional to the length of the straight-chain segments of the molecule. Kinked-conformer alkanes have LAM-type bands in this frequency region as well and several have been identified by Schaufele.[6] However, only a few of the possible conformations produce distinct Raman bands of measurable intensity, and these only in the case of the low carbon number alkanes. (In the longer liquid alkanes the multiplicity of possible gauche conformers produce bands which overlap and are indistinguishable.) Heptane has four distinct LAM-type bands of which the strongest three occur at 309 cm^{-1}, 396 cm^{-1}, and 507 cm^{-1}. Spectra of heptane at room pressure and at 14.7 kbar at 65°C are shown in Fig. 1. Our data consistently show a shift of these bands to higher frequency as a function of pressure. According to Schaufele the band at 309 cm^{-1} is the LAM due to the all-trans TTTT conformation. The band at 507 cm^{-1} results from a molecule with a single gauche bond, TGTT, and the band at 396 cm^{-1} is due to the superposition of bands from a single kink conformation, GTTT, and a double

kink conformation, TTGG.[4,6] For the longer chain alkanes in the spectral region 1060 to 1140 cm^{-1}, there is a triad of bands referred to as the optical skeletal modes. The 1060/1140 pair is associated with trans bonds and the broad band between them with gauche bonds.[7] The central band indicates the presence of chain kinking without reference to any particular gauche conformation and has been of considerable interest to biophysicists in the study of ordering in model membranes.[8] We attempted to use these bands for an indication of chain kinking under pressure in hexadecane.

Finally the region 2800 to 3000 cm^{-1} contains bands caused by the C-H stretching modes which have been shown to be sensitive to crystallinity, local ordering and chain kinking in hexadecane - again as a model for use in biophysical studies.[9] We have observed these bands for evidence of conformational changes under increasing pressure in heptane and hexadecane.

Experiment

Our samples of heptane and hexadecane were placed in small holes (1/4 mm diameter) drilled in a piece of shim molybdenum 1/4 mm thick. Diamond anvils pressing on either side of the holes sealed in the samples and compressed them to produce high pressure. A small piece of ruby was also placed in the holes so that the pressure sensitive frequency of its fluorescence peak at ~ 14400 cm^{-1} (694 nm) could be monitored to determine the pressure.

We used the 752.5 nm line of a krypton laser for the incident light. This near-ir line was chosen to reduce fluorescence from the diamonds, the ruby and the sample.[3] The beam was focused into the cell at 15° off normal

incidence to avoid specular reflection of the laser light into the spectrometer and to reduce the amount of diamond fluorescence imaged on the spectrometer slits.

Our spectrometer was a Spex 1401 with holographic gratings peaked for performance between 600 and 900 nm. Our detector was an RCA C31034A PM tube which was red-sensitive to about 900 nm.

Theory and Analysis of Data

To explain the kinking behavior of heptane we have used some concepts which have proved useful in modeling liquid crystal systems. Alben[10] has considered the statistical mechanics of a dense gas of hard rods interacting only through excluded volume effects and Van der Waals attraction. He assumed that the rods have no orientational correlations and are free to rotate end over end as in the isotropic liquid crystal case. Thus if the molecule is made more globular it sweeps out less volume as it rotates. This increases the translational entropy by reducing the excluded volume.

The important parameters of this model are the length to breadth ratio (aspect ratio) of the rod and the density. Since the alkane molecules can assume a number of conformations, the hard rod model can be extended by viewing each distinct conformation as a separate species and the liquid as a mixture of these species. Each molecule has an energy depending on the number of gauche bonds it contains and an excluded volume depending on its effective aspect ratio. Minimizing the Gibbs free energy[10] we find that conformations with lower aspect ratios (i.e. more globular) are increasingly favored as the

density is increased which is the central result of the experiment. In Fig. (2) these results are presented in a form obtained by eliminating the density as the independent variable in favor of P_o/P_o^*, where P_o is the fraction of the molecules which are all trans, and P_o^* is the value of P_o at one atmosphere. The quantity P_1 is the fraction of molecules in conformations with one gauche bond, and P_{2-4} is the fraction in conformations with 2, 3, or 4 gauche bonds.

The experimental data have been plotted in Fig. (2) under the assumption that the areas of the Raman bands change in proportion to changes in the populations of different conformers. For the data the abscissa is the ratio of the all trans band (309 cm^{-1}) at high pressure to its area at one atmosphere. The ordinate is the sum of the areas of the other three bands (356, 396 and 507 cm^{-1}) relative to the area of the band at 1450 cm^{-1} - a band which appears to be relatively insensitive to pressure. The data have been normalized to agree with the theory at room pressure.

Figure (3a) shows the area of the 309 cm^{-1} all-trans band, relative to the 1450 band, vs. pressure, and Fig. (3b) shows the all trans band, relative to the sum of the other three low frequency bands, vs. pressure. The theoretical curve is also shown in Fig. (3b) and the agreement with experiment is quite satisfactory. In this case the theoretical pressure has been deduced by comparing the theoretically predicted reduction in the all trans population with the decreases in the LAM intensity shown in Fig. (3a). Both Figs. (2) and (3) indicate that as predicted the population of unkinked and single-kinked conformers drops as the pressure rises.

Unfortunately no bands have been found which correspond to highly kinked conformations. However, the 405 cm^{-1} band which results partially from the two-kink GGTT conformation, according to Schaufele, does experience a considerable increase in intensity relative to the other low frequency bands and a leveling-off relative to the 1450 cm^{-1} band.

Spectra of the high frequency C-H stretching bands for heptane at 1 atm and at 14.7 kbar pressure are shown in Fig. (4). The intensity of the band at 2883 cm^{-1} has been correlated with the degree of chain extension and crystallinity in hexadecane.[9] The sharp decrease in the intensity of this band as the pressure rises is consistent with the kinking behavior deduced from the low frequency bands.

Similar observations of the LAM and C-H stretching spectra of hexadecane as well as the 1060-1140 cm^{-1} optical skeletal region reveal no noteworthy changes in conformational behavior. The spectra show that hexadecane in the liquid phase exists mainly in a number of gauche conformations at room pressure and that this does not change as the pressure is raised. These observations were performed in the ranges 25-165°C and 1 atm - 12 kbar pressure.

It is known that for very long chain molecules, i.e. polyethylene, that a pressure of 3 to 5 kbar induces chain straightening as the sample crystallizes from the melt.[11] Thus it might be expected that there would be a crossover value of chain length above which the kinking behavior we have observed in heptane would no longer occur.

We are now studying the longer alkanes and various polyethylenes via light scattering techniques in an attempt to observe chain straightening, if

any, that might occur at higher pressures in the fluid phases of these materials. This study may prove to be quite interesting in view of the recent reports on an ordered 'nematic'-like high pressure fluid phase of polyethylene.[12]

References

1. J. D. Barnett, S. Block and G. J. Piermarini, Rev. Sci. Inst 44: 1 (1973).
2. D. M. Adams, S. J. Payne and K. Martin, App. Spectros. 27: 377 (1973).
3. P. E. Schoen, J. M. Schnur, J. P. Sheridan, to be published in J. Appl. Spectros.
4. R. G. Snyder and J. H. Schachtschneider, Spectrochim. Acta 19: 85 (1963).
   M. Tasumi, T. Shimanouchi, and T. Miyazawa, J. Mol. Spect. 9: 269 (1962).
   R. G. Snyder, J. Chem. Phys. 47: 1316 (1967).
5. W. L. Peticolas, G. W. Hibler, J. L. Lippert, A. Peterlin, and H. Olf,
   App. Phys. Lett. 18: 87 (1971).
   R. F. Schaufele and T. Shimanouchi, J. Chem. Phys. 47: 3605 (1967).
6. R. F. Schaufele, J. Chem. Phys. 49: 4168 (1968).
7. M. Tasumi and T. Shimanouchi, and T. Miyazawa, J. Mol. Spect. 9: 269 (1962).
8. J. P. Sheridan, J. M. Schnur and P. E. Schoen (in preparation).
9. R. Faiman and K. Larsson, J. Raman Spectros. 4: 387 (1976).
   B. P. Gaber and W. L. Peticolas, Biochim. Biophys. Acta 465: 260 (1977).
10. R. Alben, Mol. Cryst. Liq. Cryst., 13: 193 (1971).
11. B. Wunderlich and T. Arakawa, J. Polymer Sci. A2: 3697 (1964).
    D. C. Bassett, Polymer 17: 460 (1976).
12. K. Monobe, Y. Fujiwara, and K. Tanaka in "Proceedings of the 4th
    International Conf. on High Press.," Kyoto (1974), J. Osugi, ed., p63,
    and K. Monobe, ibid. p865.

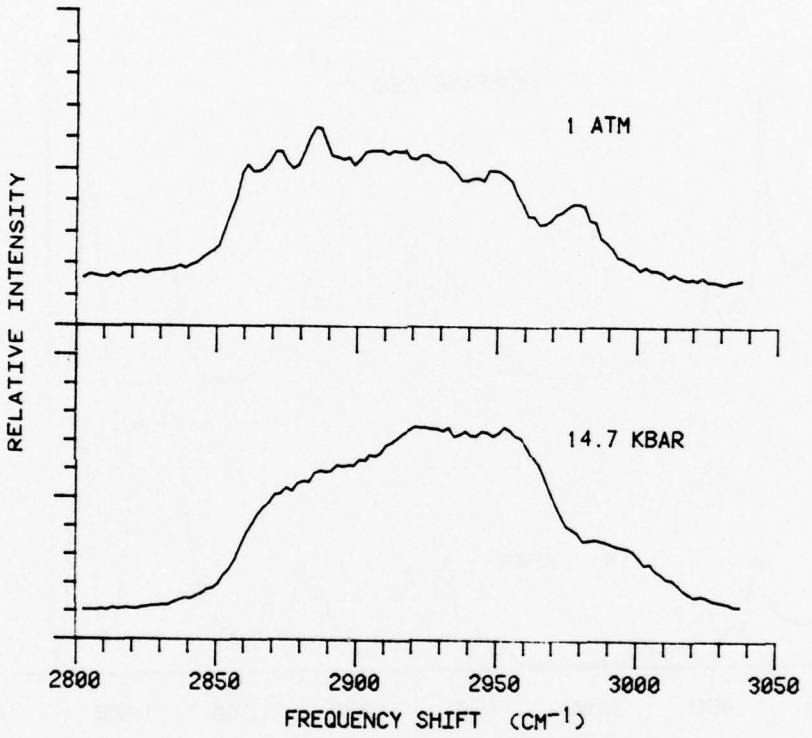

Fig. 1 — Spectra of heptane at 65°C at one atm and at 14.7 kbar

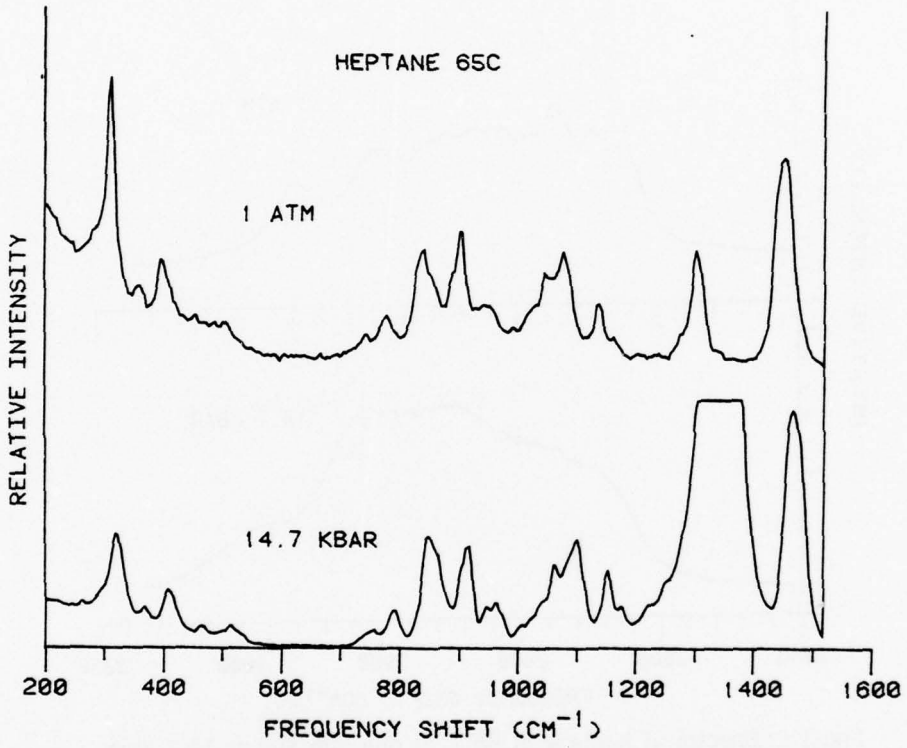

Fig. 2 — Solid lines are theoretical curves: upper line is $P_{2\text{-}4}$ vs. $P_o/P_o{}^*$ and lower curve is P_1 vs. $P_o/P_o{}^*$. θ experimental points: sum of areas of 357, 396, and 507 cm^{-1} bands (relative to 1450 cm^{-1} band) normalized to agree with theory at one atmosphere vs. area of 309 cm^{-1} band relative to its area at one atmosphere.

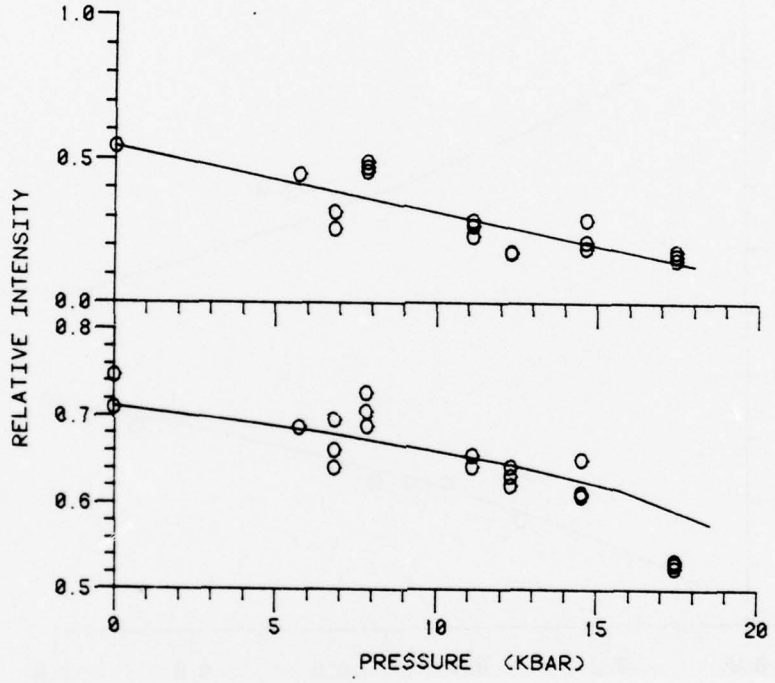

Fig. 3 — (a) θ Area of 309 cm^{-1} band relative to area of 1450 cm^{-1} band vs. pressure; solid line is least squares straight line fit to data. (b) θ Area of 309 cm^{-1} band relative to sum of areas of 375, 396 and 507 cm^{-1} bands vs. pressure; solid line is theoretical curve.

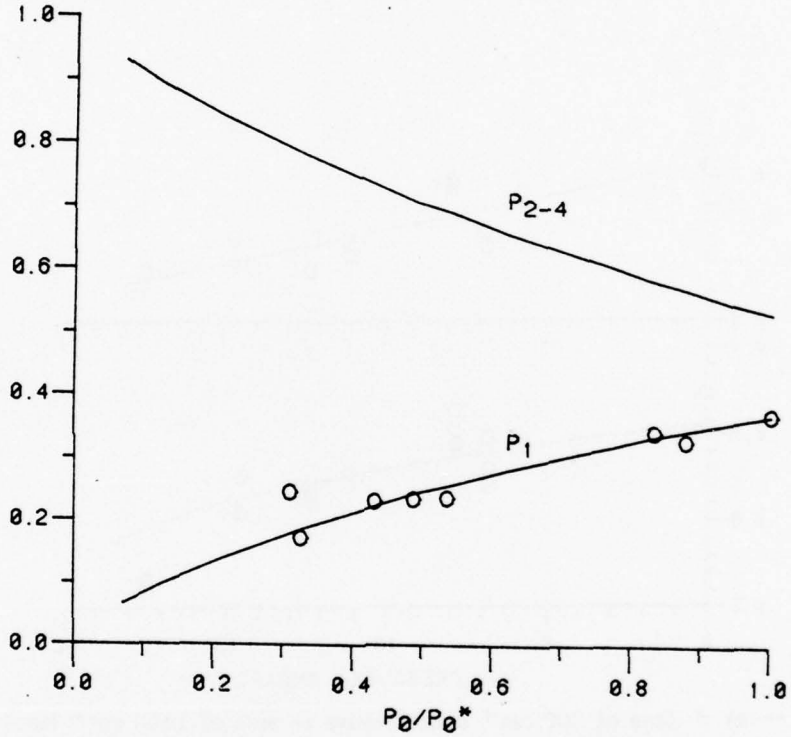

Fig. 4 — Spectra of heptane C-H stretching modes at 65°C at one atmosphere and at 14.7 kbar

(Reprinted from Nature, Vol. 270, No. 5636, pp. 412–414, December 1, 1977)

Pressure-induced changes in molecular conformation in liquid alkanes

LIQUID linear alkanes at room temperature and pressure exist in a mixture of molecular shapes. The *n*-heptane molecule, for example, has 13 possible distinct conformations with up to four gauche bonds distributed along its length. In the crystal, however, all the molecules assume the all-*trans*, straight chain shape. We have studied the conformations of chain molecules in the liquid state in various conditions using Raman scattering as a probe[1]. We have looked particularly at what happens to the shapes of linear alkane molecules subjected to high pressures in the liquid state. We speculated that as the pressure on a liquid of chain molecules was increased toward the freezing point that the chains might begin to straighten out. In fact, we found that an increase in pressure caused an increase in the number of gauche bonds, that is, pressure caused the molecules to become more globular.

Our interest in this investigation grew out of some recent discoveries concerning the conformation of linear polyethylene, a very long-chain molecule whose length can be as much as 1 μm or more. Typically, polyethylene crystallised from the melt folds itself into straight chain segments tens of nanometres long, arranged side-by-side to form lamellae, with the segment axes perpendicular to the lamellar surface. The resulting material has relatively poor mechanical strength, presumably because it is held together mainly by Van der Waals forces between lamellae rather than by the carbon–carbon bonds of the polyethylene chain. On the other hand when polyethylene is crystallised at high pressure, ~ 5 kbar, the chains are extended to their full lengths in the solid[2] and, still more interesting, there is evidence that in the high pressure liquid before crystallisation the polyethylene chains exist in a 'nematic'-like state, an ordered liquid phase[3]. We wished to investigate this ordered phase and because the spectroscopy was more straightforward, decided to begin with short chain alkanes. Our results indicate that for the short chains the ordered liquid phase does not exist.

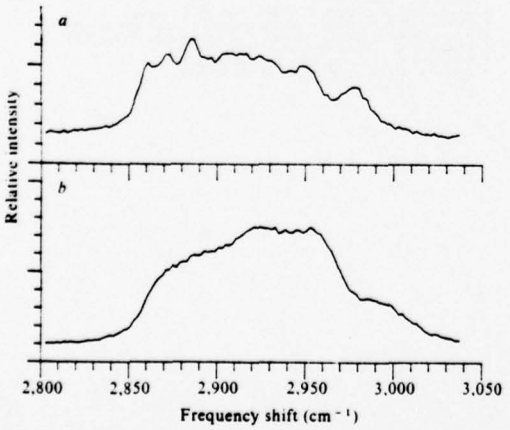

Fig. 1 The CH stretching bands for heptane at 65 °C and pressures of *a*, 1 atm and *b*, 14.7 kbar. The peak at 2,880 cm^{-1} disappears at high pressure as the molecules become more globular in shape.

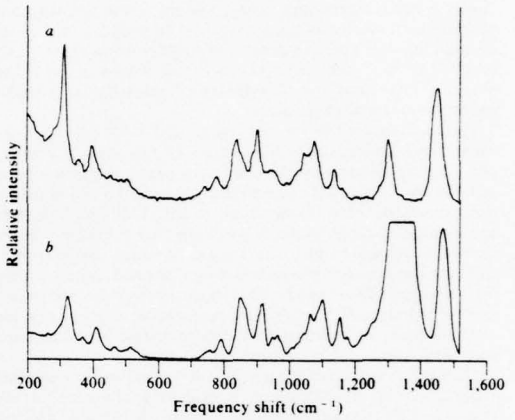

Fig. 2 Spectra of heptane as in Fig. 1 but for the lower frequency range. The intensities of the acoustic bands in the region 300–600 cm^{-1} drop as the pressure rises, indicating that the populations of molecules in the all-*trans* conformation and molecules with one gauche bond are decreasing in favour of more highly kinked conformers.

For heptane at room temperature and pressure the relative population of the all-*trans* conformer is about 15%[4]. The populations of other conformers can be calculated using the Boltzmann distribution, with each *gauche* bond requiring ~ 500 cal mol^{-1} of energy. The greater statistical weight of the *gauche* conformers overcomes the energy barrier and for liquid alkanes longer than nonane the *trans* population is small and

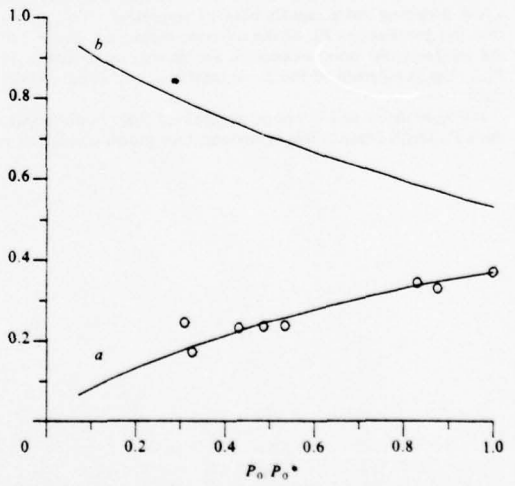

Fig. 3 Relative populations of molecules with one *gauche* bond, *a*, P_1, and with more than one *gauche* bond. *b*, P_{2-4}. The abscissa is the all-*trans* population, P_0, relative to its room pressure value, P_0^*. Pressure is increasing to the left therefore. Solid curves are theoretical predictions; open circles are data points.

spectroscopic observation of the *trans* species is extremely difficult.

In the Raman spectrum of the alkanes there are two frequency domains that are especially conformation sensitive: the high frequency C–H stretching bands and the low frequency acoustic bands. The high frequency region for heptane at 65 °C is shown in Fig. 1. The upper spectrum was taken at room pressure and shows a fairly sharp peak near 2,880 cm^{-1}, the intensity and sharpness of which has been shown to be proportional to the crystallinity and packing density of neighbouring chain molecules[3]. In the lower curve taken in the liquid at 14.7 kbar pressure this band has disappeared, indicating a probable reduction in lateral chain order.

Figure 2 shows the spectral range 200–1,500 cm^{-1} for the same two pressures for heptane. Most of this spectral range is only slightly affected by the change in pressure and the band at 1,450 cm^{-1} was used as an intensity standard. (The pressures were generated in a diamond anvil cell. The strong feature appearing in the high pressure spectrum near 1,300 cm^{-1} is the diamond Raman band.) The frequency range 300–600 cm^{-1} contains the acoustic modes which are affected quite strongly by pressure. These bands have been the subject of much study[4–7]. Model calculations have been made, and some of the normal modes for different conformations have been identified with these bands[5].

The sharp peak near 309 cm^{-1} is the so called 'longitudinal acoustic mode' (LAM) which is due to a vibration of the all-*trans*, TTTT, conformers along their chain axes. Its frequency is inversely proportional to the chain length. The band at 507 cm^{-1} results from a molecule with a single *gauche* bond, TGTT, the band at 363 cm^{-1} is due to the GTTT conformer, and the band at 396 cm^{-1} is caused by a superposition of bands from a single *gauche* bond conformation, GTTT, and a double *gauche* conformer, TTGG.

Note that in the room pressure spectrum the all-*trans* band at 309 cm^{-1} is by far the strongest peak although it accounts for only 15% of the molecular population. It seems that as the molecules become more globular in shape, vibrations along the chain length have less effect on the polarisability. The intensities of bands for 3- and 4-*gauche* bond conformers are too weak to be detected.

It is apparent from Fig. 2*b* that all the bands in the low-frequency region decrease as the pressure increases with the LAM dropping more rapidly than its neighbours. This shows that the populations P_0, of the all-*trans* molecules, and P_1, of the single-*gauche* bond molecules, are decreasing in favour of P_{2-4}, the population of the 2-, 3-, and 4-*gauche* bond conformers.

We have developed a theory, generalised from liquid-crystal theory[9], which predicts this behaviour. Our model consists of a dense gas of hard rods interacting only through excluded volume effects and Van der Waals attraction. The rods have no orientational correlations and are free to rotate end over end as in the case of an isotropic liquid crystal. Different conformers of heptane correspond to different species of rods, each with its own aspect ratio (length to breadth ratio) and energy (depending upon the number of *gauche* bonds). If the aspect ratio of a rod decreases, the excluded volume swept out as it tumbles is reduced and the translational entropy increases. If we calculate and minimise the Gibbs free energy for this model we find that rods with lower aspect ratios become more favoured as the pressure and density increase. This means that the molecules become more globular as the pressure rises.

Figure 3 shows the predictions for the rise of P_{2-4} and the drop of P_2 as functions of P_0/P_0^* (P_0^* is the room pressure value of P_0). Pressure therefore is increasing to the left in this figure. The agreement between theory and experiment is gratifying.

We have also investigated the conformational behaviour of hexane, octane, and hexadecane. The first two have behaviour similar to that of heptane. We recall that there is evidence for an ordered phase in a polyethylene liquid at high pressure. Since such a phase does not seem to exist in the short chain liquids one might expect to find a 'crossover' chain length above which the ordered phase could be found. Hexadecane at room pressure is made up almost entirely of *gauche* bonded conformers. We found that as the pressure was increased no significant change in the conformational population could be detected spectroscopically up to the freezing point for temperatures up to 165 °C. We conclude that either hexadecane is shorter than the 'crossover' length or that the ordered phase is inaccessible in this temperature range. We are continuing our investigation with other alkanes and polyethylene.

P. E. SCHOEN
R. G. PRIEST
J. P. SHERIDAN
J. M. SCHNUR

Naval Research Laboratory,
Washington, DC 20375

Received 19 August; accepted 1 October 1977.

1. Schoen, P. E., Schnur, J. M. & Sheridan, J. P. *Appl. Spectros.* **31**, 337 (1977).
2. Wunderlich, B. & Arakawa, T. *J. Polymer Sci.* **A2**, 3697 (1964).
3. Monobe, K., Fujiwara, Y. & Tanaka, I. *Proc. Conf. High Pressure* 63 and 865 (Kawakita, Kyoto, 1975).
4. Bartell, L. S. & Kohl, D. A. *J. chem. Phys.* **39**, 3097 (1963).
5. Gaber, B. P. & Peticolas, W. L. *Biochim. biophys. Acta* **465**, 260 (1977).
6. Snyder, R. G. & Schachtschneider, J. H. *Spectrochim.* **19**, 85 (1963).
7. Snyder, R. G. *J. chem. Phys.* **47**, 1316 (1967).
8. Schaufele, R. F. *J. chem. Phys.* **49**, 4168 (1968).
9. Alben, R. *Molec. Cryst. Liq. Cryst.* **13**, 193 (1971).

Printed in Great Britain by Henry Ling Ltd., at the Dorset Press, Dorchester, Dorset

A Simple Stepping Motor Programmer*

D. A. Jackson** and P. Schoen
Naval Research Laboratory
Washington, D. C. 20375

ABSTRACT

A digital stepping motor control system designed primarily for "back-lash" free repetitive scanning of a monochromator is described. It has a special feature which allows selected regions to be scanned at different rates.

* This project was supported by ONR Contract N00014-76-G-062.

** On Leave of Absence - Permanent Address: Physics Department
University of Kent
Canterbury, England

A Simple Stepping Motor Programmer

D. A. Jackson and P. Schoen

Introduction

In this paper we describe a hard-wired stepping motor programmer which is designed primarily to control a scanning monochromator. The design allows the spectrometer to be used in a multiple scan "signal-averaging mode," and is relatively simple and inexpensive, the component parts costing less than $200.00. The programmer is intended to control a TTL compatible stepping motor drive. Data is stored in a multichannel analyzer (MCA) or similar device as the stepping motor scans the spectrometer in one direction over a preset frequency range.

One of the important features of the stepping motor programmer is that its stepping rate can be altered at any point over this frequency range. This allows a detailed analysis of regions of interest in the spectrum which is particularly useful if the spectrum under investigation covers a large wavelength range with several regions containing no useful information. In this case the stepping motor drive can be programmed to scan the spectrometer slowly in the regions of interest, while data is stored in the MCA (which is stepped in synchronism with the spectrometer), and scan very rapidly through the unimportant spectral regions. At the end of the preset frequency range the direction of the stepping motor is reversed and it is stepped rapidly back to the beginning of the preset frequency range.

The position of the stepping motor shaft is determined using a simple optical method which eliminates the effects of the backlash in the gear train and enables repeated scans of the spectrometer to be made in synchronism with the MCA.

The system was tested by scanning a spectrometer over a set of Fabry-Perot channel spectra.[1] Multiple scans over lines of width ~ 0.3 cm^{-1} (spectrometer bandpass) produced no detectable line broadening.

Circuit Description

Shaft Encoder

The heart of the system is a 1024 bit random access memory (RAM) whose memory locations are made to correspond with spectrometer settings, each location separated by 10 cm^{-1}. A logical '1' is loaded into those locations at which the control decisions 'speed up' or 'slow down and take data' must be made.

In the case of our spectrometer (Spex 1401) it was convenient to use as the shaft encoder a thin aluminum disc with 10 small holes drilled on the circumference of a circle with a 36° angular separation. This disc was mounted directly on the hand crank, one revolution of which scans the spectrometer through 100 cm^{-1}. Two optical source and sensor assemblies (TIXL143) are rigidly mounted so that the aluminum disc passes through their center slots. The output of each sensor (which is TTL compatible) remains at a logic level '1', making a transition to a '0' logic level whenever one of the small holes passes through the source-sensor assembly. The sensors are positioned with an angular separation of ~ 18°.

The outputs of the sensors are connected to the preset and clear inputs of JK 1, (Fig. 1). The Q of this flip-flop is used as the counting source for both the 3 decade marker counter and the 10 bit binary counter, the outputs

of which are the memory addresses for the RAM (the additional binary counter is needed because the RAM is a binary device). The memory location selected by the binary counter is therefore always identical to the current marker counter number displayed. Both counters are negative going edge triggered. As the spectrometer scans, the output of the marker counter is compared (digitally) with the number set by thumbwheel switches which define the preset frequency range. When the number of markers scanned equals the thumbwheel setting a pulse is generated which, after being delayed by monostables (1) and (2) (see later), clears both counters. Flip-flop 3 which controls the direction of scan is also clocked by this pulse. This causes the spectrometer to scan in the reverse direction until the marker counter once again equals the thumbwheel settings. Then the direction of scan is reversed again and the whole process is repeated.

When the spectrometer is scanning in the forward direction the scanning rate is controlled by the state of JK 2 . Initially JK 2 is cleared such that the pulse rate to the stepping motor is the same as the input clock rate CK . This corresponds to the maximum'slew-rate'of the spectrometer. The stepping rate can now be altered by clocking JK 2 with the output of the RAM which has been previously programmed (see below). The stepping motor pulse rate is reduced by the number set in programmable divider 1. The ratio is variable with a maximum of 1:99. The first pulse from the RAM also externally starts the MCA allowing data to be sequentially stored in its memory. The ratio of MCA steps to stepping motor steps is controlled by programmable divider 2 which again allows the ratio to be varied up to 1:99.

Normally the RAM is programmed such that the first region of interest begins at marker count '1'. This minimizes the dead time of the system. The stepping rate is switched back to fast scan at a desired subsequent marker count by JK 2 if a logical '1' has been loaded into the corresponding RAM memory location. JK2 is clocked by the logical '1 → 0' transition of the RAM. Data collection is also inhibited by this transition. Data collection is reinitiated by the next negative-going (1 → 0) RAM output at some higher marker counter number. The RAM may be programmed to produce as many regions of interest as are required.

When the spectrometer scans up to the end of the preset frequency range JK 2 is preset to fast scan and inhibited (detail not shown in Fig. 1) from switching as the spectrometer scans rapidly back to the beginning of the frequency range.

Whenever the spectrometer changes direction the encoder remains stationary for an indeterminate time (number of stepping motor pulses), before the backlash is taken up. During this period JK 1 is preset clear as the encoder always stops at the end of the scan with optical sensor (2) illuminated. Once the backlash is taken up the encoder starts to move in the opposite direction. JK 1 is then preset high by optical sensor (1) and cleared by the next hole passing through optical sensor (2) causing the marker counter to count. This procedure eliminates both the effect of backlash (provided data collection is never initiated before marker number (1) and also prevents any false counting by the marker counter due to any multi-triggering of either optical sensor by the rather slowly moving shaft encoder. Any false counting by the marker counter will of course destroy the synchronization in the data collection.

Loading the RAM

To facilitate rapid loading of the RAM, the marker counter and the RAM counter (only) are clocked using CK . The memory is first cleared by holding both the write and data inputs of the RAM low while its driving counter is clocked up to the number equal to the full preset range set by the thumbwheels. The thumbwheels are then set to the number at which the first region of interest will commence (usually 1 for the reason stated above). One of the inputs of the NAND gate is then held at a logical '1' by the load button. The other input of the gate is fed by the comparator pulse from the marker counter. This will cause a '1' to be written into the RAM at the memory location equal to the thumbwheel setting. The thumbwheel setting is then changed to the end of the first predetermined region of interest, and a logical '1' again loaded. This procedure is repeated for every region of interest required. Monostables (1) and (2) are used in the circuit to allow sufficient time for the memory to be loaded before the reset pulse clears the memory counter to zero.

System Performance

In order to evaluate the overall performance of the programmer (coupled to the spectrometer) it is necessary to scan repeatedly over a set of well spaced spectral lines. A suitable source for this purpose is the channel spectrum produced by a Fabry-Perot illuminated with white light since it contains an infinite comb of uniformly spaced lines of adjustable linewidth. The results of scanning such a spectrum are shown in Fig. 2. The RAM has been programmed such that data is recorded in 2 regions (both 20 cm^{-1} wide) separated

by 100 cm^{-1}. The lines have ~ 6 cm^{-1} separation with ~ 0.3 cm^{-1} linewidth. The lack of degradation introduced into the data by multi-scanning over the same regions can be seen from Fig. (2). The widths of the lines in the upper trace (25 scans) are effectively identical to those recorded in a single scan (lower trace). This performance is comparable to that of commercially available computer controlled systems with the added advantage that the hard-wired unit can be built at a fraction of the cost.

References

1. F. A. Jenkins and H. E. White, "Fundamentals of Optics," (McGraw, 1959, New York) p.284.

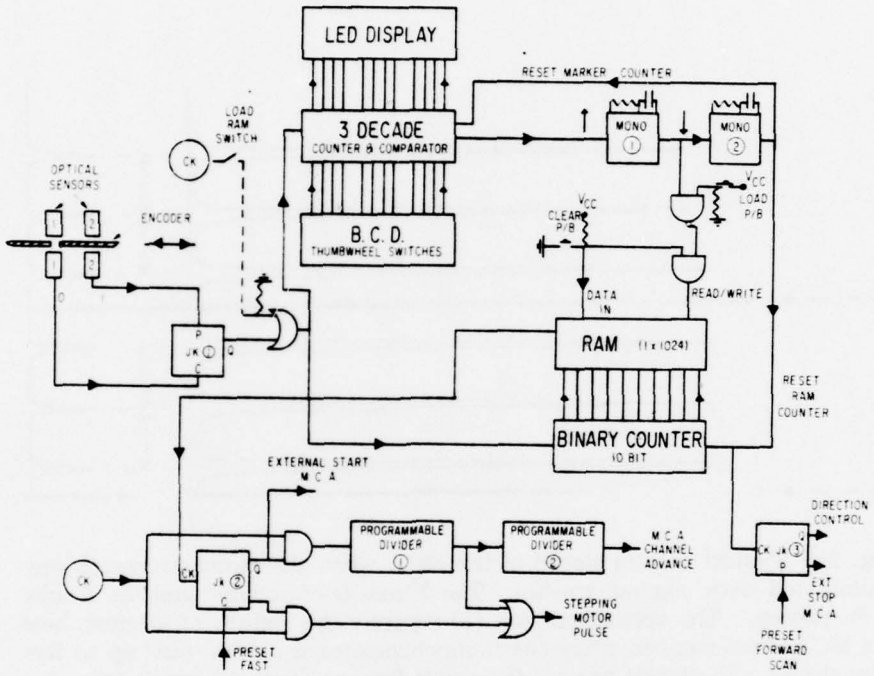

Fig. 1 — Schematic Circuit. With the exception of the RAM and the optical sensors all the integrated circuits are of the TTL 74 series. The RAM is a TTL compatible MOS 2102 (write 0, read 1).

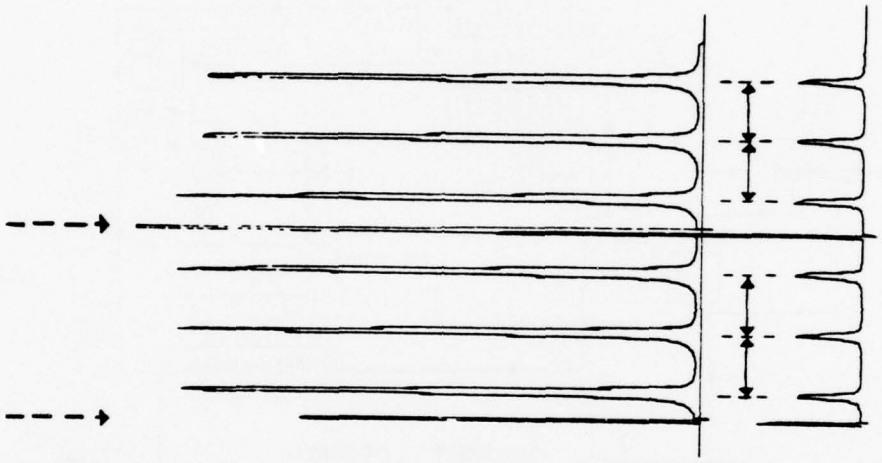

Fig. 2 — Typical spectra stored in the MCA when the monochromator was illuminated with channel spectra. The Y axis is counts/sec and the X axis is frequency. The vertical arrows (↓) separate the regions of interest, here the MCA is not stepped while the monochromator is driven 'fast' up to the next region. The lower trace is the result for one scan, the upper trace for 25 scans over the same frequency range. The separation between the two groups of channel spectra is 100 cm^{-1}, the spectral line spacing ~ 6 cm^{-1} (⟷). The ratio of forward to reverse scanning speeds is 5:1 and MCA step to motor steps 10:1.

Application of a Microcomputer to Optical Spectroscopy*

D. A. Jackson** and R. G. Priest

Naval Research Laboratory
Washington, D. C. 20375

ABSTRACT

We describe a low cost microcomputer based scanning instrument controller which has been used with both a Fabry-Perot interferometer and a grating monochromator. The system is based on a commercially available single board computer. The controller can be used in either a passive mode, where it functions as a replacement for a multichannel analyzer, or in an active control mode. Only the read only memory held program need be changed to adapt the device to a scanning instrument in either mode. Interface circuitry and typical programs are described.

*Supported by ONR Contract N00014-76-G-062

**Permanent address: University of Kent, Canterbury England

Application of a Microcomputer to Optical Spectroscopy*

D. A. Jackson** and R. G. Priest

Naval Research Laboratory
Washington, D. C. 20375

INTRODUCTION

The recent availability of sophisticated single board microcomputers has created a new option for the automation of sequential scanning instruments. Traditionally, digital data acquisition and control of instruments such as monochromators,[1-4] interferometers[5] and scanning calorimators[6] has been based on either multichannel analyzers (MCA) or minicomputers. Both of these approaches have drawbacks. The MCA is inflexible both in control and data manipulation operations. On the other hand, minicomputers require separate circuit boards for programmable clocks, for parallel ports and for serial ports in order to be useful as controllers.[7] Further, a variety of resident programming aids such as assemblers, editors and loaders are required for program development. These are difficult to use without a mass storage device such as a disk or magnetic tape. For these reasons the minicomputer based controller is costly and complex - particularly if more than one instrument is controlled by the same computer.

The single board microcomputer based controller can be both flexible and inexpensive. Its flexibility derives from its use of a stored program. Program development and testing however, are typically done on large computers of a time sharing network thus eliminating the need for associated

*Supported by ONR Contract N00014-76-G-062

**Permanent address: University of Kent, Canterbury England

equipment in the microcomputer itself. Currently available single board computers have sufficient data and program memory, ports, clocks and other features to act as instrument controllers. Although they have limited computational power microcomputers can employ virtually any communications protocol. Consequently, data obtained with a microcomputer based controller can be readily transferred to larger computers for calculations or entry into a sophisticated data base. A laboratory computer network with one large computer and a number of microcomputer based instrument controllers could be more cost-effective than a system with several minicomputers.

Our approach to the development of a single board computer based controller was to develop a system adequate for control of a vareity of instruments. In particular a Fabry-Perot interferometer and a grating monochromator have been operated with the controller we describe here. The individual characteristics of each instrument are allowed for entirely in the stored program. We chose the Intel SBC80/20 as the single board microcomputer because this device has the greatest number of features on a single board currently available.[8] This microcomputer has 4K bytes of program memory, 4K bytes of data memory , six 8-bit ports, a serial port, two programmable clocks and a vectored interrupt.

The interface circuitry for the controller includes a six decade counter, a digital display and an analog X,Y display. All of these features are capable of operation at faster than 100 microseconds per channel.

INTERFACE CIRCUITRY

The logical circuitry of the interface between the front panel connectors and the microcomputer consists of about 30 TTL integrated circuits.[9] The interface was fabricated on an Intel prototype board using wire wrap construction. The connection of this digital logic to the microcomputer is through five of the microcomputer parallel ports. Three of these ports are used by the data acquisition part of the interface for transmission of data to the microcomputer. Another of these ports is used for transmission of data from the microcomputer to the display portion of the interface. The final port is used as a set of control lines from the microcomputer to the interface. In addition, the interface is connected to two of the microcomputers interrupt lines.

The data acquisition section of the interface is based on a six decade BCD counter. There is also a 24 bit latch which can be loaded in parallel from the counter. The 24 bit latch is connected directly to the three 8 bit ports of the microcomputer which are used for data acquisition. The use of a BCD counter instead of a binary counter is possible because the microcomputer has BCD arithmetic ability. In our program numerical data are stored internally as 6 digit decimal numbers using the BCD code. This requires three 8 bit bytes per data channel. The advantage of everywhere using BCD representation for the numbers is that it is never necessary to do time consuming binary to BCD conversion for the purpose of display. This advantage offsets a slight penalty in storage efficiency.

The sequence of operations of the data acquisition section is time by a 2 microsecond clock derived from the microcomputer auxiliary clock.

The data count pulses received at a connector on the front panel reach the counter after passing through a digital gate. A data collection cycle is initiated by arrival of a pulse at the channel advance connector on the front panel. The operation sequence is then: (1) close gate to inhibit counting thus stabilizing the counter; (2) strobe contents of the counter into the latch; (3) clear the counter and open the gate. These operations result in a dead time of about 10 microseconds. The channel advance pulse is also used to interrupt the microcomputer. The interrupt latency of the microcomputer is greater than 10 microseconds so that no attempt to read the latch will be made until after the latch is stable. The operation of this circuit is shown schematically in Fig. 1.

The analog display portion of the interface is somewhat more complex. The complexity arises principally because the highest resolution integrated digital to analog converters available at reasonable cost are three digit devices whereas the data are stored as six digit numbers. Therefore, a selection of three consecutive digits out of six must be made.

It was found that program selection of the digits restricted the maximum possible scan rate of the system. This restriction was overcome using additional panel switch controlled logic circuitry.

The principle elements of the Y axis analog display section of the interface are a 16 bit shift register, a 12 bit latch and a three digit BCD integrated digital to analog converter. The X axis analog display signal is generated by a 12 bit binary counter and 10 bit binary digital

to analog converter. The lower 12 bits of the 16 bit shift register can be loaded in parallel into the 12 bit latch. The output of which is connected to the input of the DAC.

The stored data is transmitted to the shift registers via one of the eight bit ports in three sequential operations starting with the two least significant digits. The external selection lines (in conjunction with the control lines from the microcomputer) control which two of the three bytes of data are stored in the shift register and subsequently, which three of the four digits held in the shift register are displayed. The counter for the X axis DAC is also incremented during the sequence, resulting in a linear display in channel number.

In addition, control lines from the microcomputer are used to clear the X axis binary counter and to produce an end of scan signal. A position synchronization signal is also connected to a microcomputer interrupt line. These will be discussed further below.

APPLICATION PROGRAMS

The adaptation of this controller to any particular instrument is accomplished by means of the program which is placed in the microcomputer read only memory (PROM). We report here two applications which have been developed. The controller has been used as a slave device in the operation of a Fabry-Perot interferometer. In this case the controller acts as a low cost replacement for a MCA in the multiscaling mode. In the other application the controller has been used as the master control device for a grating monochromator.

Fabry-Perot Interferometer

In a previous publication[10] one of us has described electronic circuits for the generation of a voltage ramp used to control the scan of a Fabry-Perot interferometer (F.P.S.). The F.P.S. generates two signals which are routed to the microcomputer via the controller. These are a step pulse indicating that the voltage ramp activating the interferometer has advanced another unit, and a pulse indicating transmission of a strong reference peak (in this case a laser line) through the interferometer. These are used by the controller as the channel step pulse and position synchronization pulse respectively. The timing of data collection, therefore, is controlled entirely by the F.P.S. The F.P.S. can be signaled to end a scan causing the interferometer to "fly back" to its resting position and start a new scan. This signal is generated by the microcomputer as the end scan signal. The data is a series of pulses from standard photon counting electronics. The microcomputer programmable clock is not used in this application. The front panel connections are shown in Fig. 3.

The operation of the program is essentially interrupt driven. After accepting control data from a keyboard terminal and executing some initialization program steps the microcomputer waits for the position synchronization interrupt. The reception of this interrupt is the signal that data collection is to start since the Fabry-Perot has passed the position of the reference line in its scan. The program enables the channel step interrupt allowing data collection and then waits for the channel step interrupt. On receiving this signal the microcomputer reads the

three ports connected to the 24 bit latch in the interface. The six digit number read is added to the contents of the current channel data location using a three byte BCD addition alogrithm. The result is stored and sent to the display section of the interface. These operations are repeated on each channel step interrupt until the program determines that a scan is complete. Then the fly back signal pulse is sent and the channel step interrupt is disabled. Following this, the microcomputer waits for the next synchronization interrupt. Since the F.P.S. will only provide a synchronization pulse after fly back is completed and the Fabry-Perot is scanning forward, signal averaging with a real time display is achieved. The program can run at 20 scans of 512 channels each a second. This allows a steady display on an X,Y oscilloscope. A flow chart of the program is given in Fig. 4. The program occupies 250 bytes of memory while the 512 channel memory requires 1536 bytes. There are separate program segments for display (or plotting) of the memory contents while not collecting data and for transmission of data to other computers via the serial port.

Grating Monochromator

The controller has been used as the master control device in the operation of a grating monochromator (Spex 1401). The microcomputer programmable clock is used to activate the monochromator stepping motor and to act as the channel step pulse. The end scan control line is used as the direction control for the stepping motor. A slotted wheel and photodetector assembly mechanically linked to the monochromator grating drive produces a pulse

every 10 cm^{-1} of travel of the gratings. This marker pulse is used as the position synchronization pulse. The data is a series of pulses from photon counting electronics. Typically the scanning rate is slow so that the digital display can be easily read. The front panel connections used are shown in Fig. 5.

Like the Fabry-Perot program, the monochromator program is interrupt driven. Marker pulses and channel step pulses generate separate interrupts. These pulses occur asynchronously with respect to each other. The program keeps track of the number of marker pulses received. In this way it can cause the direction and speed of the scan to be changed at the appropriate times to achieve multiscan operation. The program enables the step pulse only while scanning forward and only after the first marker pulse of a forward scan has occurred. On receiving a step interrupt the microcomputer performs a data acquisition cycle similar to that of the Fabry-Perot program with the difference that data from a set number of consecutive steps is combined into a single channel. A flow chart of the program is given in Fig. 6.

The problem of backlash in the gear drive of the monochromator is eliminated in the operation of this controller because data is collected only after a marker is passed going in the forward direction. After the scan direction is changed from reverse to forward, no marker pulse will occur until after all the backlash is taken up. No problems of data registration were encountered, the overall scanning performance being comparable to that of the commercially available 'Ramacomp'[4] system.

The program could be modified to scan different regions at different rates and to allow data to be collected or ignored in these regions.

CONCLUSION

We have built an inexpensive and flexible scanning instrument controller based on a single board microcomputer. The controller has been successfully used as a MCA replacement and as an active control device.

REFERENCES

1. S. Ushioda, J. B. Valdez, W. H. Ward and A. R. Evans, Rev. Sci. Inst. 45. 479 (1974).
2. R. C. Harney and F. P. Milanovich, Rev. Sci. Inst. 46, 1047 (1975).
3. J. W. Arthur and D. T. Lockwood, J. Raman Spect. 2, 53 (1974).
4. Commercial literature available from Spex Industries, Metuchen, N.J.
5. D. A. Jackson and E. R. Pike, J. Phys. E. 1, 394 (1968).
6. Commercial literature available from Perkin Elmer Corporation, Norwalk, CT.
7. For example: PDP11 Computer Peripherals Handbook, Digital Equipment Corporation, Maynard, Mass. (1975).
8. J. Conway and P. Snigier, EDN 21, 95 (1976).
9. Circuit diagrams available on request from the authors.
10. D. A. Jackson and D. S. Bedborough, J. Phys. E. (to appear Nov. 1977).

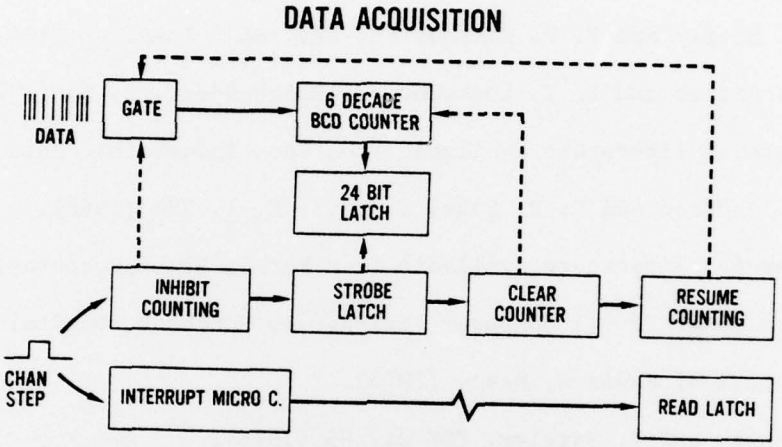

Fig. 1 — The operation and structure of the data acquisition part of the interface are shown schematically. The series of boxes pointed to by the arrows from the channel step pulse summarize the action of the device. The broken lines indicate the major elements affected by each operation.

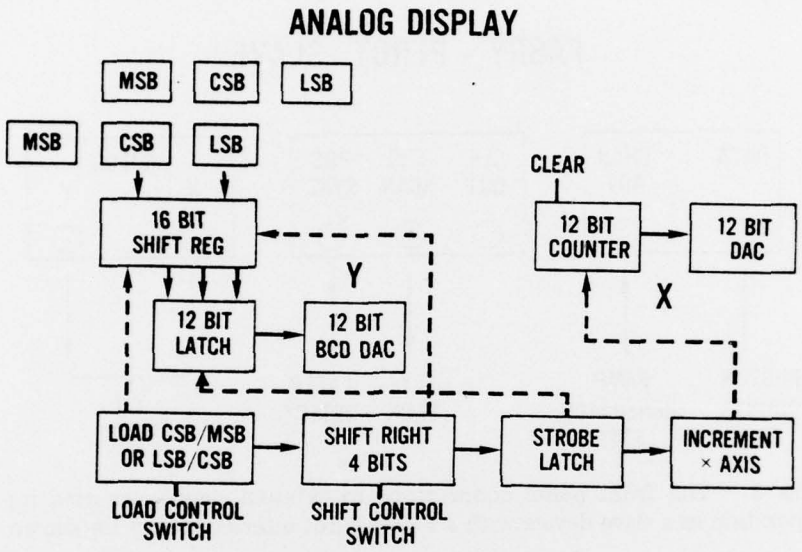

Fig. 2 — The operation and structure of the analog display part of the interface are shown schematically. The bottom row of boxes summarizes the action of the device. The broken lines indicate the major elements affected by each operation. The top left portion of the figure indicates that either the LSB and CSB or CSB and MSB of the datum are entered into the register.

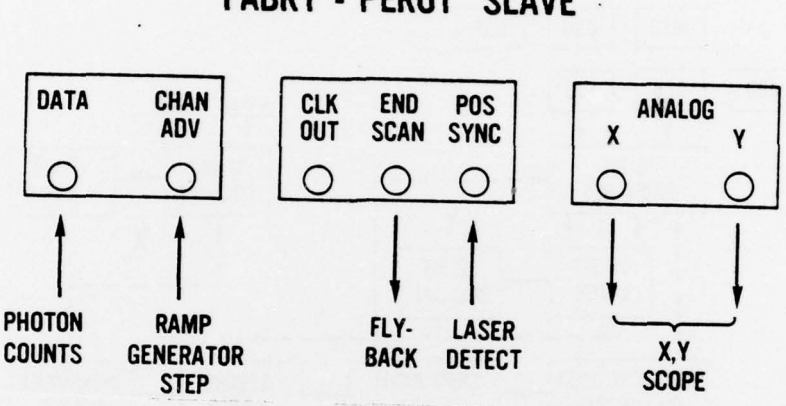

Fig. 3 — The front panel connections to external electronics used for operation as a slave device with a Fabry-Perot interferometer are shown

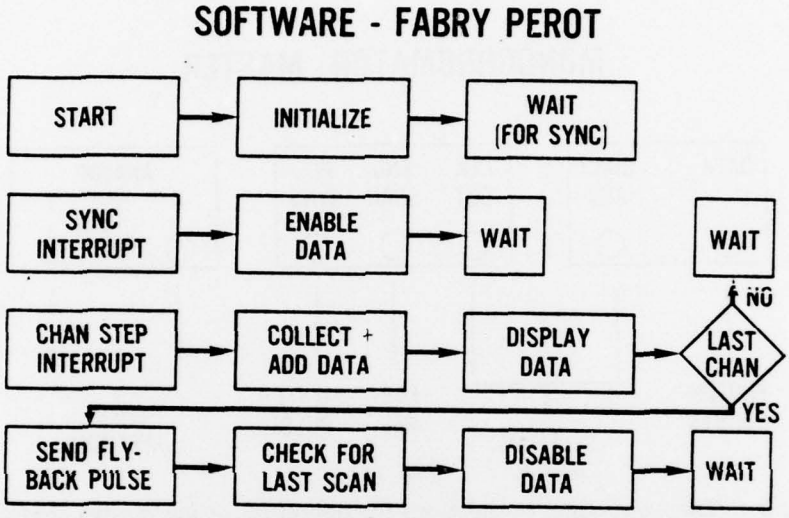

Fig. 4 — A schematic diagram of the program used with the Fabry-Perot interferometer is shown. Program control is transferred to the interrupt boxes by signals from outside the microcomputer so no arrows point to them.

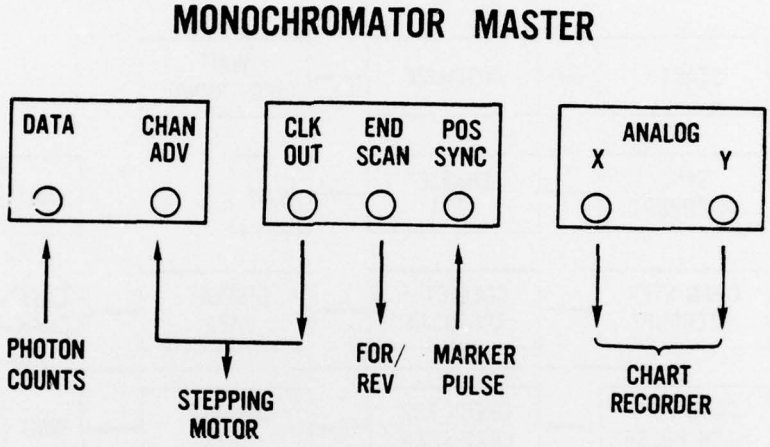

Fig. 5 — The front panel connections for operation as the master control device with a grating monochromator are shown. A marker pulse is generated every 10 cm^{-1} of grating travel by a slotted wheel connected to the grating drive.

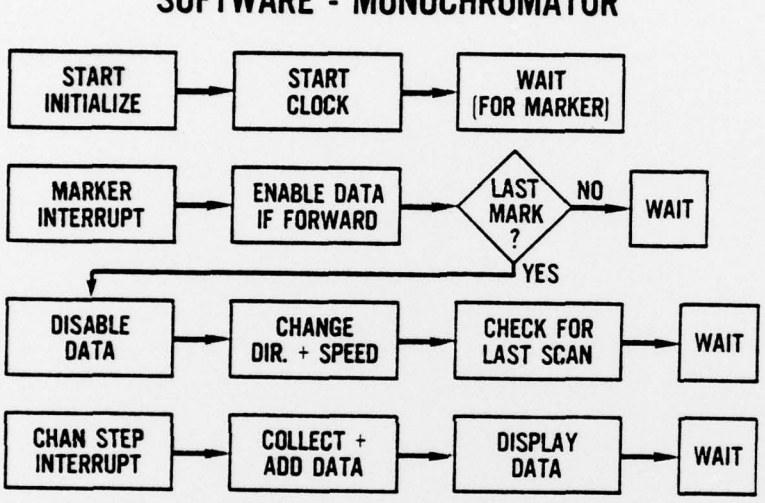

Fig. 6 — A schematic diagram of the program used with the monochromator is shown. The clock referred to is the microcomputer programmable clock.